Optimization of proprioceptive stimulation for echo-planar and inverse magnetic resonance imaging

Daniel Krahulec

School of Science

Thesis submitted for examination for the degree of Master of Science in Technology.

Espoo, 18.09.2017

Thesis supervisor:

Prof. Lauri Parkkonen

Thesis advisors:

Docent Harri Piitulainen

Docent Miika Koskinen

Aalto University
School of Science

AALTO UNIVERSITY
SCHOOL OF SCIENCE

ABSTRACT OF THE
MASTER'S THESIS

Author: Daniel Krahulec

Title: Optimization of proprioceptive stimulation for echo-planar and inverse magnetic resonance imaging

Date: 18.09.2017 Language: English Number of pages: 6+42

Department of Neuroscience and Biomedical Engineering

Professorship: Human neuroscience and –technology

Supervisor: Prof. Lauri Parkkonen

Advisors: Docent Harri Piitulainen, Docent Miika Koskinen

In echo-planar imaging (EPI), the optimal passive movement parameters (rate and duration) for studying proprioceptive brain responses are unknown. The aim of this thesis was to test the effect of stimulus rate on brain responses evoked by proprioceptive stimulation in EPI. In addition, we attempted to develop a measurement protocol for experiments focused on proprioception in ultrafast inverse magnetic resonance imaging (InI) and investigate the amplitude of blood oxygen level-dependent (BOLD) signal at varying stimulus duration. This experimental setup was supposed to be applied in future connectivity studies of the proprioceptive brain network. We found that the optimum rate for right index finger proprioceptive stimulation in EPI varies from 3 to 6 Hz. While we managed to sample the BOLD responses every 100 ms (a 20-fold increase in temporal resolution compared to EPI), the experimental design in InI is challenging due to methodological constraints. Thus, the appropriate stimulation parameters for InI still remain a topic for further research.

Keywords: fMRI, ultrafast magnetic resonance imaging, proprioception, sensory stimulation, passive movements, somatosensory cortex

Preface

This study was conducted at Advanced Magnetic Imaging (AMI) Centre and at the Department of Neuroscience and Biomedical Engineering, Aalto University. I would like to express my gratitude to all members of the research team for their indispensable helpfulness, invaluable assistance and active participation in bringing the study to a successful end. In particular, I would like to thank my advisors, Dr. Harri Piitulainen and Dr. Miika Koskinen, and my supervisor, Prof. Lauri Parkkonen, for their active comments and thorough attitude towards correcting the thesis during its completion. Likewise, my thanks belong to Timo Nurmi for his technical and analytical support. Special thanks belong to Toni Auranen, Marita Kattelus and Tuomas Toivonen for their guidance in the measurement setup and implementation of the brand-new technology. Finally, yet importantly, I want to thank my family and peers for their support and encouragement they have shown during my studies.

Otaniemi, 18.09.2017

Daniel Krahulec

Contents

Abstract ii

Preface iii

Contents iv

Symbols and abbreviations vi

1 Introduction 1

2 Background 3
2.1 Physiological background . . . 3
2.1.1 Proprioception . . . 3
2.1.2 Proprioceptive stimulation in MRI . . . 3
2.1.3 Stimulation rate and stimulus duration . . . 4
2.1.4 Proprioceptive stimulation of upper limbs . . . 5
2.1.5 Proprioceptive stimulation of lower limbs . . . 7
2.2 MR imaging sequences . . . 9
2.2.1 Echo-planar and inverse MR imaging . . . 9
2.2.2 Block design . . . 11
2.2.3 Event-related design . . . 11
2.3 Research questions and hypotheses . . . 12

3 Research material and methods 13
3.1 Subjects and experimental design . . . 13
3.1.1 Subjects . . . 13
3.1.2 Equipment for proprioceptive stimulation . . . 14
3.1.3 Study protocol . . . 14
3.1.4 Block design in EPI . . . 15
3.1.5 Event-related design in InI . . . 16
3.2 Data processing . . . 21
3.3 Statistical analysis . . . 23

4 Results 24
4.1 EPI study . . . 24
4.1.1 Cortical location of the main responses . . . 24
4.1.2 Average response strength . . . 24
4.2 InI pilot studies . . . 28
4.2.1 Cortical location of the main responses in study 1 & 2 . . . 28

5 Discussion **30**
5.1 EPI study 30
5.1.1 Cortical location of the main responses 30
5.1.2 Average response strength 30
5.2 InI pilot studies 31
5.2.1 Cortical location of the main responses in study 1 & 2 31
5.3 Limitations and future prospects 32

6 Conclusions **33**

Appendices **34**

References **36**

Symbols and abbreviations

ANOVA	analysis of variance
BD	block design
BOLD	blood oxygen level-dependent contrast in fMRI
CP	cerebral palsy
CPM	continuous passive movement
CT	computed tomography
D	contrast matrix
ECG	electrocardiogram
EEG	electroencephalography
EPI	echo-planar imaging
ERD	event-related design
FDR	false discovery rate
FIR	finite impulse response
fMRI	functional magnetic resonance imaging
FOV	field of view
FWER	family-wise error rate
FWHM	full width at half maximum
GEEPI	Gradient-Echo Echo-Planar-Imaging
GLM	general linear model
GRAPPA	GeneRalized Autocalibrating Partial Parallel Acquisition
HDR	hemodynamic response
HRF	hemodynamic response function
InI	inverse imaging
M1	primary motor cortex
MEG	magnetoencephalography
MPRAGE	Magnetization-Prepared Rapid-Acquisition-Gradient-Echo
N	number of subjects
N_t	number of trials
$\vec{p}$	vector with trigger onset timings
PAT	parallel acquision technique
PET	positron emission tomography
PMCMR	Pairwise Multiple Comparisons of Mean Rank Sums (an R package)
ROI	region of interest
S1	primary somatosensory cortex
S2	secondary somatosensory cortex
SMA	supplementary motor area
SMC	primary sensorimotor cortex
SMG	supramarginal gyrus
SNR	signal-to-noise ratio
SPM	Statistical Parametric Mapping (MATLAB toolbox)
T_1	spin-lattice relaxation time
T_2	spin-spin relaxation time
T_2^*	time constant characterizing the exponential decrease in signal strength after spin excitation by a radiofrequency pulse
T_A	acquisition time
T_E	echo time
T_R	repetition time
VBM	voxel-based morphometry

1 Introduction

Brain imaging encompasses a set of tools to directly or indirectly draw inference about structural and functional properties of the nervous system. By the nineteenth century, scientists started to pursue the idea that the human brain consists of distinct areas that support different cognitive processes. Early attempts examined the anatomical surface of the skull to infer about the underlying cortical volume. However, these methods lacked exact scientific basis and were quickly abandoned.

Improved evidence about the gross organization of the brain was obtained from cases of brain damage (mostly in animals), which provided important insights about characterizing neurological disorders. Nevertheless, animal studies did not suffice for unravelling complex brain functions and due to ethical reasons, invasive measurements on humans were prohibited. Thus, non-invasive neuroimaging methods started to be developed. Today, the most frequently used non-invasive brain imaging techniques include magnetoencephalography (MEG), electroencephalography (EEG), optical imaging, positron emission tomography (PET), computed tomography (CT), voxel-based morphometry (VBM), functional magnetic resonance imaging (fMRI), and structural MRI.

Unlike in CT and PET, fMRI has the advantage of avoiding the use of X-rays. Moreover, fMRI produces images with small voxel size (even 1 mm). Brain function can be evaluated safely, effectively and at practically no risks.

In comparison to MEG or EEG, the sampling rate of fMRI is lower due to the sluggishness of the hemodynamic response (peaking at approx. 5 s after neuronal firing occurs in a brain area and lasting for ∼20 s). In addition, the fMRI signal only represents an indirect measure of neuronal activity based on the blood oxygenation level and therefore the signal magnitude can be influenced by non-neuronal changes in the body, paramagnetic effects, and by compensation for oxygen consumption by increased blood flow (Glover, 2011, Huettel et al., 2014). In fact, the electrophysiological basis of the BOLD signal is obscured by the poorly understood nature of neurovascular coupling.

Most fMRI techniques exploit the susceptibility effects of paramagnetic contrast agents (e.g. gadolinium or dysprosium) or oxyhemoglobin (BOLD imaging) to acquire imaging contrast (Ogawa et al., 1990). During task-evoked brain activation in fMRI experiments, the focal cerebral arterial oxyhemoglobin levels are changing. As long as the arterial blood propagates into veins, the T_2^* relaxation time of the venous blood is transiently prolonged, thus increasing signal intensity on T_2^*-weighted images.

The principal pulse sequence applied in diffusion, perfusion or functional MRI has been echo-planar imaging (Cohen and Schmitt, 2012). However, due to the low temporal resolution of typically ∼2 s in EPI, it is difficult to precisely sample the hemodynamic responses with respect to their occurrence in different regions of interest (ROIs) (Lin et al., 2014). Faster sampling may allow for the detection of subtle differences in the onsets of BOLD activity among brain regions, which is why an ultrafast inverse magnetic resonance imaging (InI) sequence has been developed (Lin et al., 2012b).

We exploited this brand-new technology in event-related design (ERD) and assessed its applicability in exploring the spatiotemporal structure of the somatosensory areas that are activated by proprioceptive stimulation.

Proprioception is the ability of specialised sensory receptors (proprioceptors) to control the position and movement of different body parts in space. Proprioceptive stimulation refers to a scientific method for studying the functional properties of proprioception by stimulating the brain via proprioceptive afference (i.e. ascending neuronal pathways propagating from the periphery via thalamus to the cortex).

Findings from stroke-affected humans have shown that passive movements activate the sensorimotor cortex more than any other movement paradigm (e.g. active movements or motor imagery) (Szameitat et al., 2012). We aimed at developing a stimulation protocol that could be applied in neurorehabilitation. Hence, we applied passive movements of the limbs to facilitate proprioceptive stimulation. The stimuli were delivered to the subjects via pneumatic artificial muscles, to which the stimulated body parts (an index finger and a foot) were attached.

In humans, sensorimotor integration and its coupling with proprioceptive afference have not yet been fully understood. Even less is known about brain mechanisms related to proprioception in humans with neurological diseases. Knowledge of the underlying physiological mechanisms in proprioceptive deficits is crucial for treatment planning, as experimental paradigms with proprioceptive stimulation can better elucidate abnormalities in the sensorimotor integration of the brain (Ciccarelli et al., 2005), and help select suitable rehabilitation methods for patients.

First neuroimaging examinations of humans with impaired proprioception have shown that proprioceptive stimulation with passive movements used in neurorehabilitation is beneficial for the retention of motor function (Carel et al., 2000, Mintzopoulos et al., 2008, Takahashi et al., 2008), improves the control of sitting balance in chronic stroke survivors (Luca et al., 2017), and causes cortical reorganization of functional connectivity in Parkinsonian patients (Baradaran et al., 2013). Little is also known about proprioceptive deficits in cerebral palsy (CP), which is associated with motion instability (Katz-Leurer et al., 2014, Hung and Meredith, 2014) as well as in cerebral infarction (Fu et al., 2015, Lee et al., 2012). Proprioceptive stimulation may even be utilized in the recovery process of other motor disorders, such as chorea or dystonia, which have rarely been investigated in the context of proprioception (Abbruzzese et al., 2014, Deuschl et al., 1989, Rosenkranz et al., 2009).

We strived to elucidate, which stimulus rate is optimal for studying proprioceptive brain responses in EPI. Our next aim was to design an experimental protocol for proprioceptive stimulation in InI, where we additionally tested the effect of varying stimulus duration on the magnitude of somatosensory responses.

The dataset used in this thesis was acquired on a 3.0T MR scanner (Siemens Skyra, AMI Centre, Aalto University). The following sections provide an insight into the physiological principles of proprioception and methods for proprioceptive stimulation in fMRI.

2 Background

This section provides an overview of both historical, recent, and contemporary investigative approaches employed in available studies of proprioception.

2.1 Physiological background

First, the functional characterization of proprioception is explained. Next, several outcomes from previous studies applying proprioceptive stimulation of upper and lower limbs in neuroimaging are presented.

2.1.1 Proprioception

In the human sensory perception, energy is transduced from one form (light, pressure, temperature) to electrochemical energy in the form of action potentials (other forms are also possible). This type of transduction is mediated via sensory receptors.

The term 'proprioception' describes the function of specialized sensory receptors (proprioceptors) that inform the brain how the body is positioned and moving in space. These movement sensors are embedded in muscles (muscle spindles, tendon organs), joints (joint receptors), and in connective and soft tissues of the locomotor system (Enoka, 2015). They are sensitive to changes in the position of limbs, movement direction, and force magnitude (exerted by limbs) (Bear et al., 2015).

In the following chapters, primary attention is paid to the functional aspects of proprioceptively stimulated brain activations.

2.1.2 Proprioceptive stimulation in MRI

Historically, neuroscience has experienced a transition from analyses of endogenous oscillations and evoked responses in EEG towards network-level connectivity analysis, resting state fluctuations, multivariate analyses, and the overall aim to localize signal sources from MEG and fMRI data (Bandettini, 2009). Rapid advancement of neuroimaging methodology has allowed for obtaining data with better spatial resolution to study functional dynamics, structural locations, and diverse types of brain activity.

Various tools have been employed to investigate the human sensorimotor cortex. Until the late 90s, PET (Mima et al., 1999, Weiller et al., 1996), EEG and MEG had mainly been used for this purpose. For instance, many brain oscillations recorded by EEG (Wilke et al., 2009) and MEG (Hinkley et al., 2007) have been compared to fMRI hemodynamic changes to localize the sources of activity in order to find correlations between these methodologies.

To stimulate the somatosensory cortex, complementary investigative methods such as event-related evoked potentials (ERPs) (Alary et al., 1998), electrical stimulators with electromyography (EMG) guidance (Francis et al., 2009) or transcranial magnetic stimulation (TMS) (Wilke et al., 2009) have additionally been implemented to the study protocols.

Emerging clinical studies on motor disorders have proposed promising improvements in limb movement control after patients underwent proprioceptive training using e.g. vibrations (Ben-Shabat et al., 2015). Both in fMRI, MEG and EEG, proprioceptors have typically been stimulated by passively moving the limbs to evoke cortical responses. Such stimulation demands the use of specialized equipment, such as MRI-compatible mechatronic robots (Van de Winckel et al., 2013), pneumatic actuators (Belforte and Eula, 2012), manually controlled mechanical manipulanda (Ciccarelli et al., 2005) or pneumatic artifical muscles (Piitulainen et al., 2015).

The following subsections provide an insight into what has been experimentally investigated in fMRI with proprioceptive stimulation applied both to upper and lower body extremities.

2.1.3 Stimulation rate and stimulus duration

Our attention is paid to proprioceptive stimulation using passive movements of the limbs in fMRI. A vast majority of studies investigating brain responses to proprioceptive stimuli used similar experimental paradigm. Investigators performing proprioceptive stimulation have typically been guided by acoustic cues (Ciccarelli et al., 2005) or visual cues (Ben-Shabat et al., 2015) to facilitate aimed timing of the stimulation.

Proprioceptive stimulation of the limbs has often been conducted at the rate of approximately 1 Hz (Alary et al., 1998, Ben-Shabat et al., 2015, Boscolo Galazzo et al., 2014, Carel et al., 2000, Dinomais et al., 2009, Guzzetta et al., 2007, Hinkley et al., 2007, Sahyoun et al., 2004, Van de Winckel et al., 2013, Veverka et al., 2016, Ward et al., 2006) or below 1 Hz (Blatow et al., 2011, Ciccarelli et al., 2005, Iandolo et al., 2015, Lee et al., 1998, Vér et al., 2016).

However, no available study has yet precisely stated the empirical reason for the choice of stimulation rate in experiments involving passive movements. In general, the rate has typically been selected given the circumstances of the experiment, e.g. sustaining comfortable movement range, peak velocity of the device or ensuring a sufficient number of stimuli within the time constraints of the measurement. In lower limb stimulation, the passive movement rate has also been set similar to that of ankle dorsiflexion movements when walking at casual velocity (Francis et al., 2009).

Moreover, the effect of stimulus duration for proprioceptive stimulation in MR InI has never been studied before.

In the following subsections, we describe past paradigms with proprioceptive stimulation using passive movements of both upper and lower limbs solely in fMRI.

2.1.4 Proprioceptive stimulation of upper limbs

Over the last two decades, experimental conditions with passive movements of different parts of the upper extremities have typically been applied in fMRI to explore activation patterns and functional connectivity in the human brain.

Proprioceptive input is sequentially processed through the lower somatosensory cortex (contralateral Rolandic area with respect to the stimulated limb) and then simultaneously in the supplementary motor area (SMA) and the inferior parietal lobe, see Fig. 1 (Alary et al., 1998).

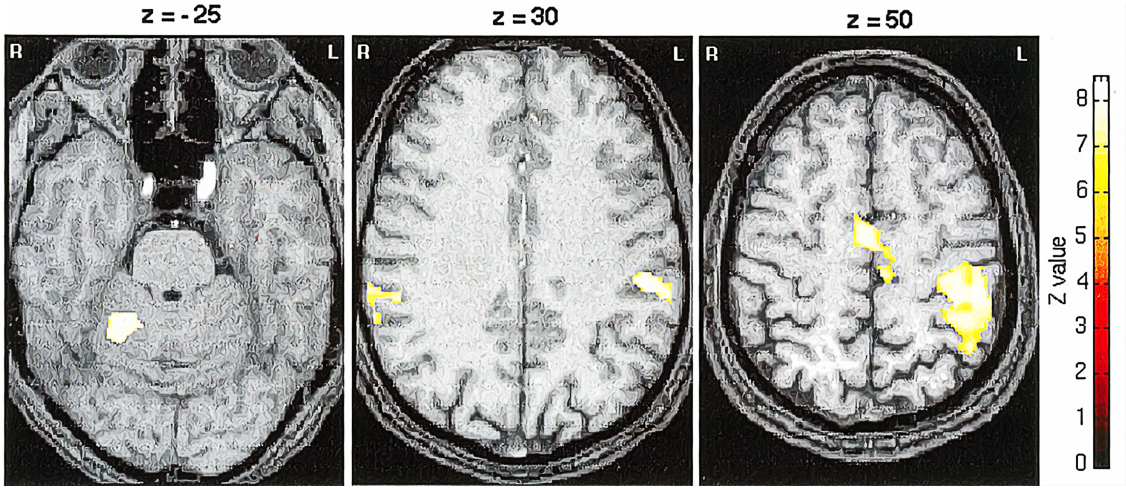

Figure 1: SPM t-maps converted to z-maps of passive right wrist extension in 6 subjects. *Left*: ipsilateral cerebellum; *center*: bilateral inferior parietal lobes; *right*: contralateral primary somatosensory cortex (S1), premotor cortex, and SMA. Z-scores indicate distance in millimeters with reference to the intercomissural line, which is at 0 mm (Alary et al., 1998).

Repeated passive flexion-extension of the wrist has been a part of most rehabilitation procedures in patients with motor deficits. The sensorimotor network was scrutinized under fMRI before and after a 4-week repetitive proprioceptive training by passive movements that were delivered by an operator (Carel et al., 2000). Training-induced cortical plasticity is depicted in Fig. 2. The post-training analysis showed activity and reorganization of activation patterns in areas responsible for motor planning, namely the contralateral primary sensorimotor cortex (SMC) and the 'SMA proper' region, referring to the posterior part of the supplementary motor area, which is responsible for the execution of both simple and complex movements. These changes in plasticity were rendered a neural basis for neurorehabilitation.

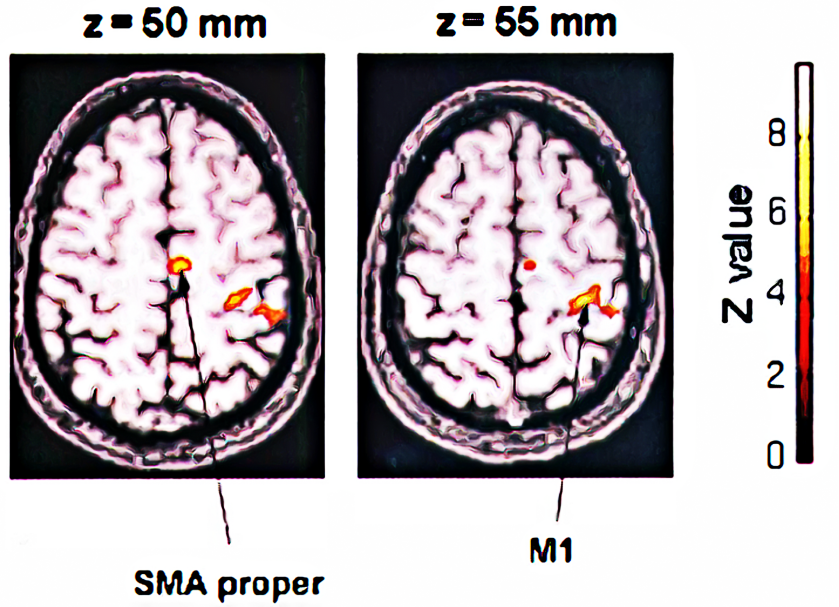

Figure 2: Changes in plasticity after the 4-week passive movement training. Activation maps of statistical differences between outcomes from the post- and pre-training fMRI examinations of data from six volunteers. The Z number refers to the distance in mm with respect to the intercomissural line as a reference at 0 mm (Carel et al., 2000).

Experience with the application of passive motor training for the recovery of the ability to perform active movements in patients with brain glioma (Blatow et al., 2011) has confirmed the significant role of primary motor cortex (M1). Patients with brain tumor can thus benefit from proprioceptive stimuli in the form of passive movements in clinics (see Fig. 3).

Further experiments have suggested that decreased proprioception could be associated with decreased function of the right supramarginal gyrus (SMG) and dorsal premotor cortex, which plays a key role in spatial processing and motor control (Ben-Shabat et al., 2015). Decreased SMG function may be related to proprioceptive deficits in cases of right hemispheric lesions.

In CP patients, a notable emphasis has been put on the importance of the right postcentral gyrus (Van de Winckel et al., 2013). In this research study, an MR-compatible robot was passively stimulating children's fingers, and responses to passive movements were compared to active movements and tactile stimulation. Results are shown in Fig. 4.

Although it had previously been stated that there was a connection between the somatosensory cortex and the ipsilateral cerebellar area in CP-affected children (Wilke et al., 2009), the study by Van de Winckel et al. (2013) found ipsilateral activation of the cerebellum only in typically developed (TD) children. This difference was explained by the fact that robotic initialization of passive movements does not evoke almost any brain responses in the cerebellum unlike when conducted by an operator.

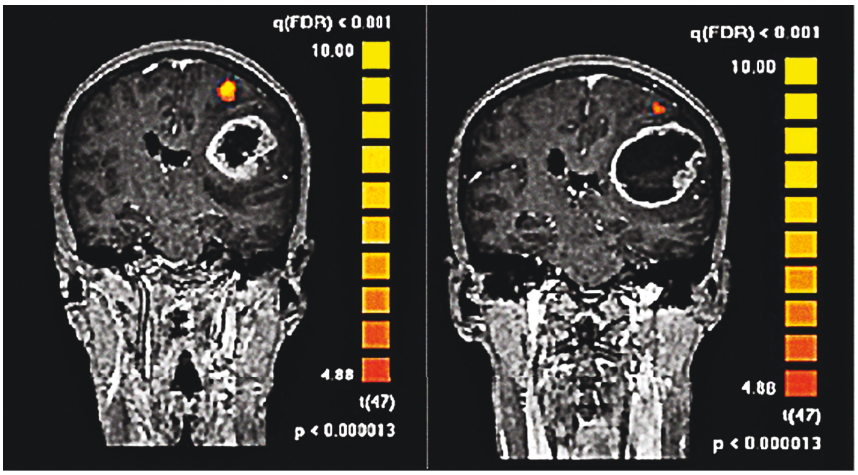

Figure 3: Clinical fMRI with passive motor stimulation (Blatow et al., 2011). *Left*: the main activation in the M1 area; *right*: coactivation in the S1 hand area. Centroids indicate areas with highest statistical power. P-values were corrected for multiple comparisons using false discovery rate (activations with FDR < 0.05 are visualized here).

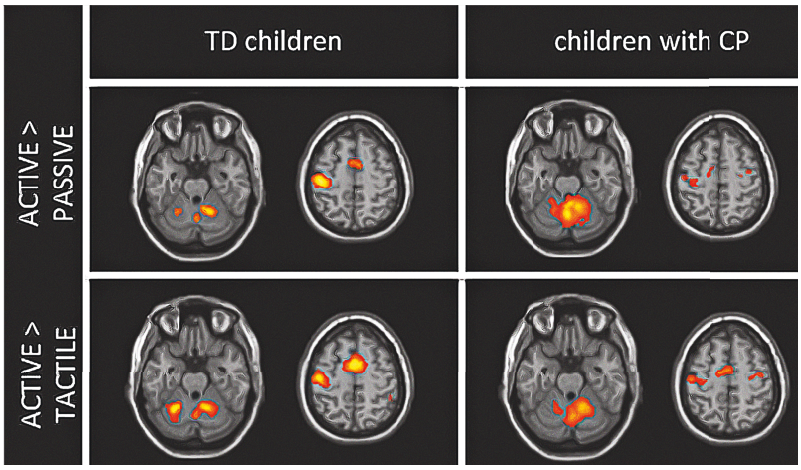

Figure 4: T-statistics (from a 2-sample t-test) in the form of colormaps to observe main differences between active movements and passive movements as well as active tactile movements. The t-values are scaled from 0 to 10. The voxel clusters (encompassing more than 10 voxels) represent significant activations corrected at FDR < 0.05 (Van de Winckel et al., 2013).

2.1.5 Proprioceptive stimulation of lower limbs

Concerning lower-limb proprioceptive stimulation in fMRI, there are fewer reports on activations evoked by passive movements of the lower extremities compared to proprioceptive stimulations of upper limbs.

Brain responses to proprioceptive stimulation using passive movements of the lower limbs are more widely spread across the sensorimotor cortex, as opposed to active movements (Sahyoun et al., 2004, Ciccarelli et al., 2005).

Passive foot movements are associated with activations in the sensory and motor cortex of the left hemisphere, which corresponds to the areas of activation evoked by passive hand movements. However, in the reverse contrast (i.e. active vs. passive movements), findings have provided evidence for activations in the cerebellum, thalamus and putamen (see Fig. 5).

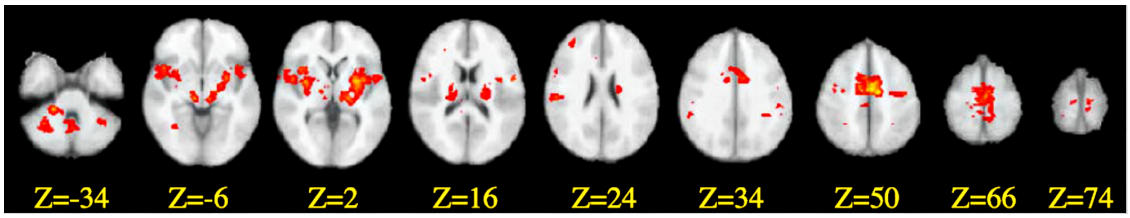

Figure 5: Contrast maps of the active vs. passive movement conditions. Anatomical lateralization: left hemisphere on the left, right hemisphere on the right. Z-scores are thresholded at $Z > 1.8$ with a cluster threshold at p-values < 0.05 (Sahyoun et al., 2004).

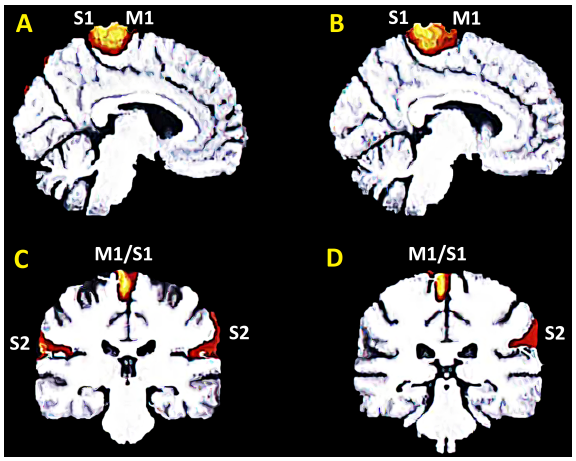

Figure 6: Brain activations on T1-weighted images. Both in healthy (*right column*) and paretic (*left column*) subjects, the CPM stimuli activated areas M1 and S1 (A, B). In both groups, there was an ipsilateral activation in the secondary somatosensory cortex (S2) (C, D), while only in the CPM training of paretic-ankle also contralaterally (Vér et al., 2016).

Ankle-foot continuous passive movement (CPM) device therapy significantly improves the passive range of motion of the ankle and efficiently decreases the spasticity in the early phase of rehabilitation (Vér et al., 2016). Brain responses to CPM are shown in Fig. 6.

2.2 MR imaging sequences

We applied two fMRI sequences, namely EPI and InI. The latter sequence was used with the intention to detect the timing of BOLD responses with better accuracy.

As one of the oldest techniques for spatial localization in MRI, EPI was first described by Mansfield in 1977 (Mansfield, 1977). First imaging with EPI was done in the early 1980s, when Mansfield's group produced biologic images of an infant human heart.

InI is a novel ultrafast sequence for fMRI, developed to reveal more information about temporal dynamics of the brain activity (Lin et al., 2006, 2012b). Below, the principles of the design of both fMRI sequences are presented, and fMRI experimental designs are introduced.

2.2.1 Echo-planar and inverse MR imaging

Echo-planar imaging has found diverse applications in functional brain mapping, particularly in localization of brain activity. EPI provides functional MRI with decreased sensitivity to motion and fast acquisition speed (Edelman et al., 2005). Latest variations of two-dimensional EPI (single/multi-shot EPI) enable to acquire a single-slice T_2^*-weighted images in approx. 80 ms, which allows for whole-head coverage in 1—3 s with 3mm isotropic resolution (Lin et al., 2006). In three-dimensional imaging, standard single-shot EPI can achieve a spatial resolution of 1—6 mm (Lin et al., 2012b).

In recent years, new fMRI sequences have started to be developed with the aim to detect fast physiological changes and subtle neuronal activations in BOLD fMRI data. It has been objected that the sluggishness of the hemodynamic response hampers the detection of rapid brain dynamics, even if the sampling rate of fMRI is improved. Nevertheless, scanning only a few slices with EPI (Menon et al., 1998) or adding jittered stimulus timing to enhance the sampling rate have been adjustments that succeeded in finding differences of BOLD onset times within hundreds of milliseconds (Penny et al., 2011).

Recently, parallel MRI techniques, such as SMASH (Sodickson and Manning, 1997) or GRAPPA (Griswold et al., 2002) have accelerated MR acquisition by collecting data through multichannel receiver coil arrays. However, despite many advantages of parallel MRI, e.g. reduction of gradient-switching noise (de Zwart et al., 2004) or cancellation of ghosting artifacts (Kellman and McVeigh, 2001), its speed is limited by the low number of channels in head coil arrays (a constraint mathematically described as an over-determined linear system). High-channel head coils (consisting of 64 channels) have been developed to increase the acceleration of parallel imaging 64-fold (McDougall and Wright, 2005).

InI is inspired by essential similarities between deriving spatial information in MRI (i.e. gradient encoding) with a 90-channel head coil array and in MEG (i.e. the geometrical distribution of magnetometers) (Hämäläinen et al., 1993).

While EPI uses a slow slice-selective gradient to perform partition encoding, InI gathers spatial information by simultaneous acquisition of data about the radiofrequency field (B_1) distribution from multiple channels in the head coil array. In InI, dynamic changes are spatially resolved with statistics by solving an inverse problem, which is analogous to MEG/EEG source localization (Fig. 7). In practice, InI reconstruction uses reference scan data to derive spatial information. Thus, faster acquisition is facilitated by replacing time-consuming spatial encoding, dependent upon gradient switching, with an alternative approach utilizing an image reconstruction algorithm. Currently, using a 32-channel head coil array, MR InI offers a 100 ms sampling rate with whole-brain coverage (Chang et al., 2013).

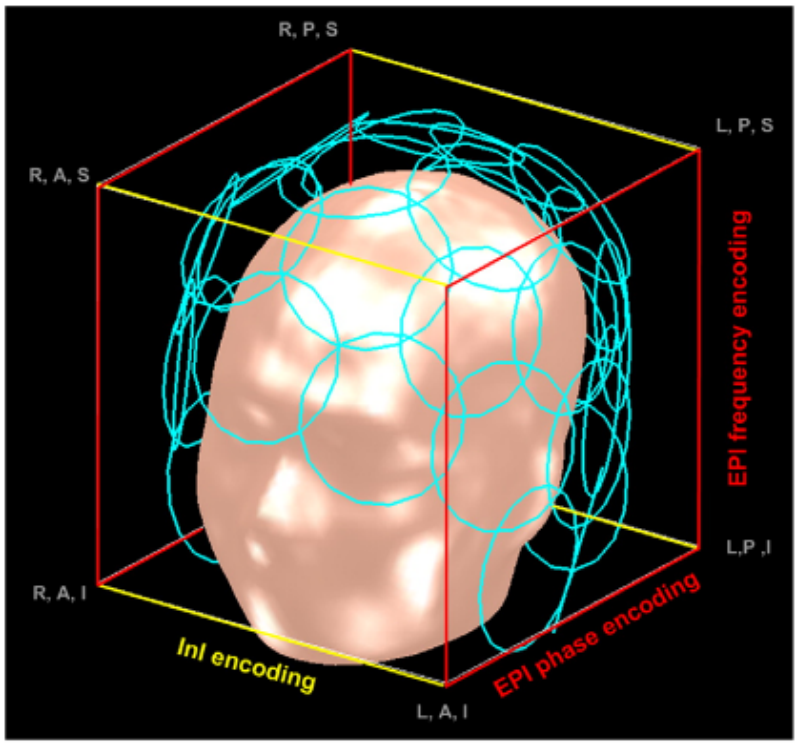

Figure 7: Visualization of the three-dimensional InI spatial encoding method using a 32-channel head coil. In-plane encoding is performed by EPI's frequency- and phase-encoding gradients, while spatial information is derived by solving an inverse problem based on minimum-norm estimates. Orientation: L = left, R = right, A = anterior, P = posterior, S = superior, I = inferior (Lin et al., 2008).

Since InI is a relatively new technique, its use poses specific challenges regarding the sustainability of high spatial resolution at high sampling rate. A modification of InI (echo-shifting) allows the repetition time (T_R) to become smaller than the echo-time (T_E). Consequently, this technique can measure one whole-brain volume per 25 ms, while keeping high spatial resolution and less than 2-fold temporal SNR loss (Chang et al., 2013). In general, the spatial resolution in InI increases with longer distance from the center of the brain (20 mm) towards the cortex (5 mm).

Several applications of InI have been reported. Although its spatial resolution is slightly decreased in one encoding direction, the acquisition speed can be exploited in dynamic imaging, such as resolving timing delays of hemodynamic responses at neuronal scales (Lin et al., 2010), improving the detectability of BOLD responses (Krüger and Glover, 2001) or inferring causality among brain areas (Deshpande et al., 2010). For instance, InI has allowed for detecting feed-forward causal modulations in a BOLD fMRI study on visuomotor reaction time (Lin et al., 2014).

In 3T fMRI experiments, InI can be advantageous in physiological noise suppression. It has been found that 33 % of the total physiological interference in BOLD signals is caused by cardiac and respiratory effects (Birn et al., 2006). Echo-planar imaging requires ∼2 s to image the whole brain, which is why high-frequency physiological noise cannot be suppressed using this MR imaging technique. By contrast, the high temporal sampling rates achievable with InI permit extensive reductions in physiological noise, which leads to improved estimation of the hemodynamic response (Lin et al., 2012a). Nevertheless, external monitoring of the breathing and cardiac activity is desired to suppress the temporal aliasing of noise.

2.2.2 Block design

In the past, fMRI experimental designs were born as identical clones of those currently being used in PET, where the response of many adjacent successive trials is averaged over a short period, typically 15—50 s (Dale and Buckner, 1997). Block designs (BD) allowed for establishing either task-specific or mixed task conditions, depending on the nature of trials. BDs are inherently suitable for assigning ROIs to particular tasks (Bandettini, 2009, Donaldson, 2004), which was beneficial for our study.

BDs also suffer from fundamental limitations. Firstly, this experimental construct is not able to estimate the frequency of erroneously occurring trials within a block (Taylor et al., 2007). Moreover, BDs cannot distinguish between positive and adverse responses within a block, which results in averaging both response types and reduces the amplitude of brain activity (Meltzer et al., 2008).

2.2.3 Event-related design

Compelling evidence based on experience with BDs has confirmed that neuronal activity could be extracted from evoked hemodynamic responses (HDR) (Petersen and Dubis, 2012). In ERDs, it is assumed that neural activity occurs for short and discrete intervals. Seeing that high temporal resolution is regarded as the essential property of ERDs, random order (jittering) of trials is usually applied to avoid temporal correlations between successive stimuli (D'Esposito et al., 1999).

The advantages of ERDs are reflected in better estimation of the shape and timing of the HDR, event randomization (Tie et al., 2009), and avoidance of trial predictability (Petersen and Dubis, 2012). On the other hand, these designs also have downsides. The detection power of ERDs is weaker than in BDs, as their experimental efficiency is proportional to the number of events that are averaged. Moreover, ERDs are susceptible to artifacts arising from non-physiological signal fluctuations (Miezin et al., 2000).

We utilized a 'slow' and 'rapid' ERD. With slow ERDs, the stimulus events are spaced far apart so that their hemodynamic response functions do not overlap and return to baseline before the next trial begins. Conversely, in rapid ERDs, individual trials are spaced at short intervals (as short as 2 s), which causes that the hemodynamic response does not completely revert back to the signal baseline.

2.3 Research questions and hypotheses

Our aims were to determine the appropriate stimulus rate to maximize the proprioceptive responses in EPI, create a measurement protocol for proprioceptive stimulation in InI, and test the effect of rate and different stimulus durations on proprioceptive responses in InI.

To achieve these aims, we tried to quantify the brain response strength. Also, we conducted source analysis using visualisation software (the MNE toolbox and SPM package) to assess the spatial distribution of brain activation on the cortical surface.

Our research questions and hypotheses were:

Q_1: Is it possible to find a precise stimulus rate, at which the proprioceptive BOLD responses to passive movements are the strongest in EPI?

H_1: Based on previous MEG results (Piitulainen et al., 2015), we expected to see the strongest proprioceptive BOLD responses at the stimulus rates ranging from 3 to 6 Hz which corresponds to the upper limits of natural movement.

Q_2: Are we able to record proprioceptive BOLD responses using InI?

H_2: We assumed that we are able to detect the shape of the hemodynamic response to passive movements in the primary somatosensory cortex using InI.

3 Research material and methods

This section introduces the methodologies employed in this study and explains our experimental protocols. Also, the choice of subjects, sequence parameters, and equipment for proprioceptive stimulation are discussed.

3.1 Subjects and experimental design

First, an explanation of the study protocol and the experimental setup is given in this subsection. Then, details about our BD and ERD are described.

3.1.1 Subjects

For the EPI study, we recruited a total of 10 healthy adults, while in both InI studies, 2 healthy adults participated altogether. A strict criterion in subject selection was right-hand dominance, as proprioceptive stimulation was applied to the right upper and lower limbs. All subjects filled out safety questionnaires to check that MRI is not harmful to them, thereby preventing any deterioration of the MR signal by metallic implants or other MR-incompatible items. Metal detectors were used for this purpose.

Figure 8: Subject placement on the patient table with attached pneumatic actuators before the actual measurement.

3.1.2 Equipment for proprioceptive stimulation

To execute passive movements of upper limbs in our experiments, we have assembled two MR-compatible movement actuators. The devices were constructed from an artificial muscle that shrinks with increasing air pressure (delivered to the instrument in a tube, see Fig. 9a). It is a replica of an MEG-compatible actuator modified for the use in MR scanning (Piitulainen et al., 2015). Moreover, the device can easily be attached to the patient table of the scanner using plastic nuts and bolts.

Similarly, data collection from lower-limb movement stimulation has been performed using a newly-developed MR-compatible device with electro-pneumatic control (Fig. 9b). These devices are constructed so that smooth ankle dorsiflexion ($\sim$15°) is ensured. The physical working principle is the same as in the hand devices described above. Of great importance is fixation of the measured subject on the table, tight strapping of the feet as well as immobilization of the device itself.

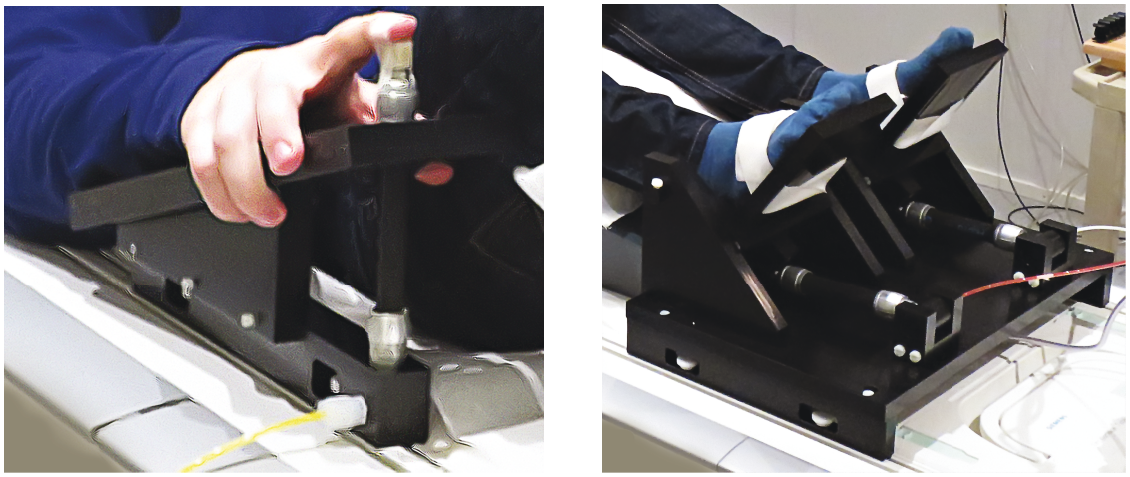

(a) (b)

Figure 9: fMRI pneumatic device for (a) hands and (b) legs.

3.1.3 Study protocol

During the scanning, subjects were instructed to remain as still as possible. When placing them on the patient table (Fig. 8), particular attention was paid to correct positioning of the pneumatic actuators for proper stimulation.

Accelerometers were utilized to track the movement kinematics of the actuator in different stimulation rates. Simultaneously, we recorded pulsation with a pulse oximeter attached to the index finger of the unstimulated hand and the breathing curve. In addition, electrocardiogram (ECG) was recorded in InI measurements. However, the quality of the ECG signal was low due to superimposed noise that originated from rapid gradient switching. Physiological signals were recorded by BIOPAC at a sampling rate of 1 kHz. All recording components were attached to a portable tray next to the patient table.

During the EPI acquisition, the subjects were instructed to fix their gaze to a black cross situated at the distantly projected computer screen (on a mirror) above their head. Conversely, during the InI measurements, space images were shown to the subjects. In either of the cases, it was important to avoid excitations in the visual cortex, as such unintended stimulation would have led to improper localization of brain activations.

3.1.4 Block design in EPI

In our EPI measurements, we applied a BD (Fig. 10) with six conditions (passive movements at different rates, see Tab. 1) and a resting state condition intercepting every stimulus condition. Two functional runs were obtained and each run consisted of 6 blocks. Each block included all 6 conditions, rest being the initial one. The experiment was run using a Gradient-Echo Echo-Planar-Imaging (GEEPI) sequence (parameters in Tab. 2). Individual high-resolution T_1-weighted structural three-dimensional (3D)-MRI datasets were acquired using a Magnetization-Prepared Rapid-Acquisition-Gradient-Echo (MPRAGE) sequence.

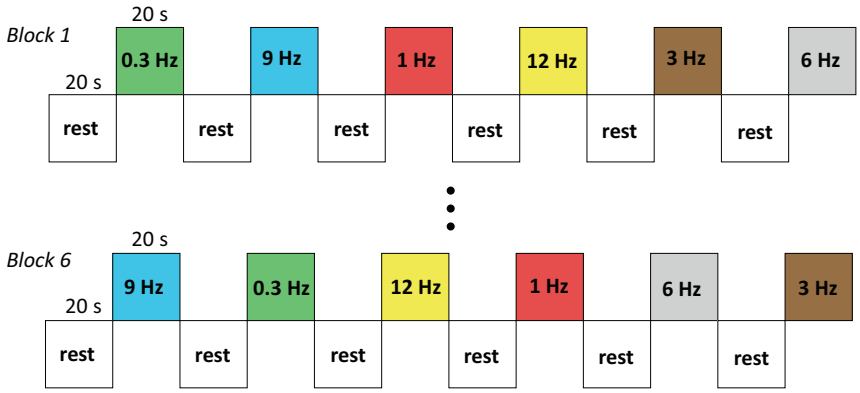

Figure 10: Block design for the EPI experiment in one functional run.

Condition (Hz)	Trigger pulse duration (ms)	Block length (s)
0.3	200	20
1.0	200	20
3.0	120	20
6.0	70	20
9.0	50	20
12.0	36	20
Rest	–	20

Table 1. Parameters of the block design.

	Functional GEEPI	Anatomical MPRAGE
T_A	5 min 8 s	6 min 2 s
T_R	2500 ms	2530 ms
T_E	30 ms	3.30 ms
FOV	192 × 192 mm	256 × 256 mm
Slice thickness	3.0 ms	1.0 ms
Base resolution	64 × 64	256 × 256
Bandwidth	2442 Hz/px	200 Hz/px
FA	90°	7°
Number of slices	44 axial	176 saggital
PAT mode	GRAPPA	GRAPPA
Voxel size	3.0 × 3.0 × 3.0 mm	1.0 × 1.0 × 1.0 mm
Fat suppression	fat saturation	none

Table 2. Imaging parameters for the EPI protocol.

3.1.5 Event-related design in InI

Experimental designs for both InI studies are schemed in Fig. 11. Based on our experience, the continuous acquisition time in each run was limited to 5 minutes (in InI pilot study 1) and 3 minutes (in InI pilot study 2) to mitigate the effects of magnetic inhomogeneities. Stimulation parameters were chosen based on results from the EPI experiment (Tab. 3). The measurement parameters were adjusted with the aim to optimize the SNR and collect more trials (Tab. 4).

In the InI pilot study 1, we used a slow ERD with fixed stimulus interval and randomized presentation of stimuli. We mainly aimed at observing the magnitude and shape of the average hemodynamic response, which is why we set the stimulus interval to 12 s without any jitter. We further assumed that increasing the length of runs would allow us to obtain enough stimulations. The exact length of each run in the first InI study was approximately 5 min 20 s.

However, after the data from the first study was analyzed, the signals were highly corrupted with noise and the signal magnitude was quite low. Therefore, in the InI pilot study 2, we applied a rapid ERD with a stimulus onset asynchrony (jitter) varying from 4 to 12 s. We further decided on reducing the acquisition time down to 3 min 5 s per run. Unlike in the first study, we recorded 8 functional runs with the stimulation of the right hand index finger, and 4 runs with passive movements of the right ankle to understand whether we can detect brain activations evoked by leg stimulation.

Modifications were applied to the number of stimuli, the length of stimulus interval, and the number of runs. In Tab. 5, the sequence parameters are listed. These settings were not changed after the first study. The experiment was run using a Gradient-Echo Echo-Planar-Imaging (GEEPI) sequence. Individual high-resolution T_1-weighted structural 3D-MRI datasets were acquired using a Magnetization-Prepared Rapid-Acquisition-Gradient-Echo (MPRAGE) sequence.

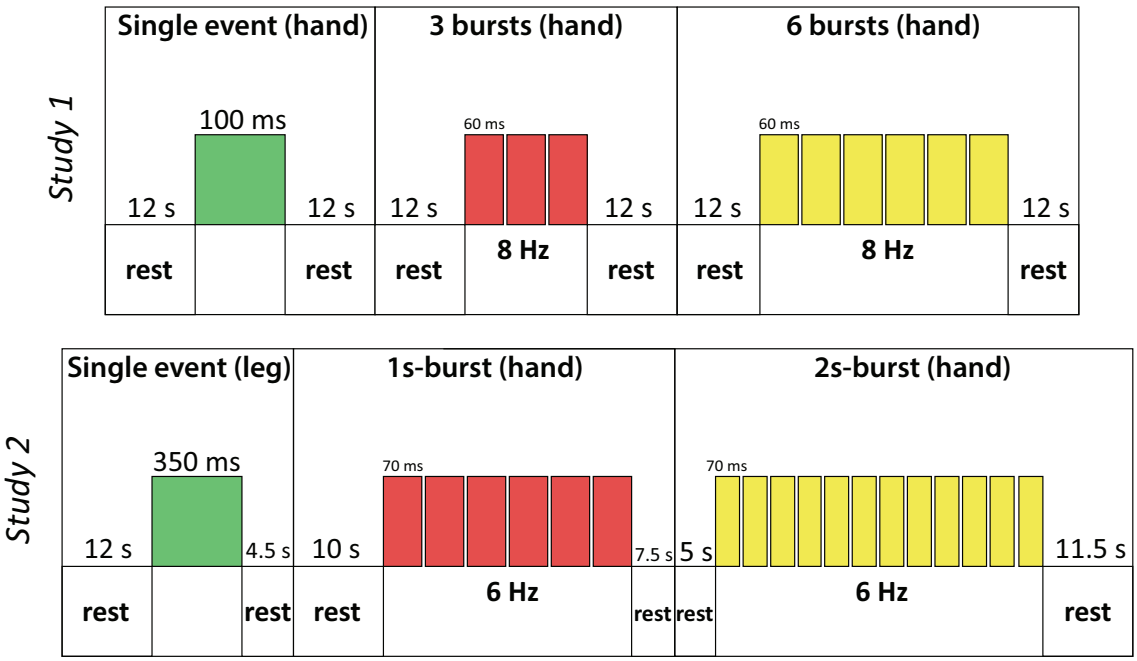

Figure 11: Diagrams of the ERD for InI pilot study 1 with regular stimulus interval and InI pilot study 2 with stimulus onset asynchrony. In study 1, the 3- and 6-burst stimuli were 375 ms and 750 ms long, respectively. In study 2, we doubled the number of bursts in both stimulus conditions and decreased the stimulus rate from 8 to 6 Hz.

Condition 1 – runs 1, 4, 7: single events	
Stimulus interval	12 s
Pulse duration	100 ms
Number of stimuli per run	75
Condition 2 – runs 2, 5, 8: several bursts	
Stimulus interval	12 s
Stimulus rate	8 Hz with 3 consecutive biphasic movements
Movement duration	375 ms
Pulse duration	60 ms
Number of stimuli per run	75
Condition 3 – runs 3, 6, 9: several bursts	
Stimulus interval	12 s
Stimulus rate	8 Hz with 6 consecutive biphasic movements
Movement duration	750 ms
Pulse duration	60 ms
Number of stimuli per run	75
Summary	
Total number of stimuli	225
Total duration of the functional part	∼45 min
Anatomical T_1	∼7 min
Coil shimming	9 min (9× 1 min)
Reference scans	2 min 15 s (9× 15 s)
Total duration of experiment	∼1 h 3 min 15 s

Table 3. List of parameters in the InI pilot study 1 (right hand index finger stimulated).

Condition 1 – runs 1, 4, 7, 10: single events	
Stimulus interval	4—12 s
Pulse duration	350 ms
Number of stimuli per run	88 (22 per run)
Condition 2 – runs 2, 5, 8, 11: several bursts	
Stimulus interval	4—12 s
Stimulus rate	6 Hz with 6 consecutive biphasic movements
Movement duration	1000 ms
Pulse duration	70 ms
Number of stimuli per run	88
Condition 3 – runs 3, 6, 9, 12: several bursts	
Stimulus interval	4—12 s
Stimulus rate	6 Hz with 12 consecutive biphasic movements
Movement duration	2000 ms
Pulse duration	70 ms
Number of stimuli per run	88
Summary	
Total number of stimuli	264
Total duration of the functional part	∼37 min
Anatomical T_1	∼7 min
Coil shimming	12 min (12× 1 min)
Reference scans	3 min (12× 15 s)
Total duration of experiment	∼59 min

Table 4. List of parameters in the InI pilot study 2. The right ankle was stimulated in condition 1 and the right hand index finger in conditions 2 and 3.

	Functional InI	Anatomical MPRAGE
T_A	5 min 20 s	6 min 2 s
T_R	50 ms (2-segment scan)	2530 ms
T_E	27.50 ms	3.30 ms
FOV	210 × 210 mm	256 × 256 mm
Slice thickness	7.0 ms	1.0 ms
Base resolution	42 × 42	256 × 256
Bandwidth	3970 Hz/px	200 Hz/px
FA	25°	7°
Number of slices	24 axial	176 saggital
PAT mode	none	GRAPPA
Voxel size	5.0 × 5.0 × 7.0 mm	1.0 × 1.0 × 1.0 mm
Fat suppression	fat saturation	none

Table 5. Imaging parameters for both InI protocols.

3.2 Data processing

EPI data was sampled at $T_R = 2.5\,\text{s}$, and consisted of 44 slices per each subject, the duration of each task run was 25 min 8 s, and the length of the localizer scan was 5 min 8 s. Both the anatomical and functional data were processed with Matlab 2016b and the SPM12 (Statistical Parametric Mapping) toolbox. The anatomical T_1-weighted images were reconstructed using FreeSurfer.

First, the EPI data was preprocessed in the following steps:

1. slice-timing correction applied to different slices
2. motion correction to compensate for voxel-wise motion artifacts
3. unwarping to account for image distortions due to magnetic field inhomogeneity
4. normalization to transform EPI images of the subjects into an anatomical space
5. spatiotemporal smooting of functional images with a Gaussian kernel with 6 mm full width at half maximum (FWHM) to increase SNR
6. functional data were filtered with a temporal high-pass filter of 754 s for the actual experimental run and 154 s for the functional localizer run

Second, the trigger timings were extracted and a standard general linear model (GLM) analysis performed:

1. extracting trigger onset times, event types and movement regressors with a block duration of 20 s
2. constructing a design matrix with all event types, onsets and durations
3. convolving the design matrix with a canonical hemodynamic response function
4. performing subject-wise GLM analysis

Third, SPM contrast vectors were constructed for individual subjects, where ones were assigned to the regressor of the only condition of the functional localizer. Next, using the Marsbar toolkit, the ROIs were extracted according to the SPM contrast activation maps.

After the GLM analysis, we calculated the grand-average of all time-courses. We extracted the time-courses modelled by finite impulse response (FIR) basis function for each individual, condition, and ROI. The time-courses were averaged over all voxels separately for S1 and S2, and visualised in a 40s long time window, depicting the percentage signal change with respect to the baseline level.

Within each ROI, we averaged the β-values for all voxels, and calculated the mean β-values over all subjects for each stimulus condition. Average peak response values were extracted subject-wise from the average time-series in each ROI.

Last, using FreeSurfer, we obtained a template subject for cortical surface representation (a grand-average of cortical surfaces was performed with a smoothing kernel of 20 mm). Subsequently, group-level GLM analysis was conducted. We used custom Matlab scripts with SPM12 functions to build t-statistic maps of cortical activations.

InI data was sampled at $T_{\mathrm{R}} = 100\,\mathrm{ms}$, and consisted of 24 slices per each subject. Each functional run was recorded in 5 min 20 s (InI study 1 with 9 runs), and 3 min 5 s (InI study 2 with 12 runs). Both image reconstruction algorithms and statistical analysis procedures were implemented with Matlab. For InI reconstruction, we collected reference scans before each functional run, in order to gain information about the entire three-dimensional volume. Savitzky-Golay low-pass filtering (order 1, framelength 20.1 s) was used to smooth and detrend the signal as well as to discard the scanner drift. Then we estimated the hemodynamic response function (HRF) in each projection image across all channels of the coil array.

The spatial co-registration between InI reconstructed data and the anatomical data was done in FreeSurfer. Then, the co-registration matrix was applied to each time instant of the InI hemodynamic response to transform the neural activity estimates for each functional run onto an inflated cortical surface space. The transformed results were also spatially smoothed with a 3D Gaussian kernel with 10mm FWHM.

From a list of stimulus onset times, we constructed a vector $\vec{p}$ with entries containing ones that indicate the occurrence of stimuli at the stimulus onset times, and all other entries containing zeros. A contrast matrix D was created from the convolution between the $\vec{p}$ vector and the hemodynamic response function H,

$$D = \vec{p} * H\,, \tag{1}$$

where the asterisk denotes the convolution. We used a finite-impulse response (FIR) basis for the HRF. H modelled an HRF of 30 s duration with a 6 s pre-stimulus baseline.

The design matrix was appended with two confound vectors (linear drift and constant confounds). Additionally, the spatial grand-average time series was used as a confound. Least squares fitting was applied for the estimation of GLM coefficients for all channels at all time instants.

To allow statistical inference from the results of the InI time-series reconstruction, dynamic statistical parametric maps (dSPM) were derived as the time-point by time-point ratio between the effect of particular time-points and the baseline noise level, which is represented by the standard deviation of the pre-stimulus interval. Estimating the effects of 30 s in steps of 100 ms with 6s pre-stimulus interval, we obtained 300 effect estimates. Taking a ratio between each of these 300 estimates and the noise level estimate (standard deviation of the estimates during the 6s pre-stimulus interval) allowed for generating 300 dSPMs.

The statistical significance of dSPM was approximated as t-statistics. Under the null hypothesis of no hemodynamic response, dSPMs should be t-distributed. The t-statistics of the evoked hemodynamic response were calculated for each image voxel at each time instant. The exact threshold for these t-statistics was difficult to determine, as there is no analytical model about the baseline fluctuation regarding its degree of freedom.

Last, the BOLD signal strength and the t-statistics of the evoked hemodynamic responses were visualised over the whole brain using the MNE toolbox.

3.3 Statistical analysis

GLM β-values and the mean peak values of average brain responses were tested for statistical significance.

Parametric statistical tests require the data to be normally distributed. We decided to use a non-parametric statistical test corresponding to repeated measures ANOVA, namely the Friedman two-way analysis of variance by ranks, because we recorded data from a relatively low number of subjects ($N = 10$) – see the normality test results in Table 6.

Friedman test allows for greatly improved detectability of differences in variables by dividing subjects into homogeneous subgroups and performing within-subject comparisons in these subgroups (in our case trials, $N_\mathrm{t} = 6$). A disadvantage of the parametric freedom is reflected in the loss of statistical power of Friedman test, compared to the parametric ANOVA versions (Hollander and Wolfe, 1999).

When comparing across repeated measures, the hypotheses for comparisons were defined as:

H_0: The average β-values and the mean peak values of average responses do not differ across conditions.

H_1: The average β-values and the mean peak values of average responses differ in some conditions.

To arrive at correct conclusions about significant between-group differences based on the mean rank, post-hoc tests have been developed. As the Friedman test indicates significance (e.g. $\chi^2(5) = 23.57, p < 0.01$), it is meaningful to conduct statistical tests for multiple comparisons to identify exact locations of the differences between the groups. Several tests have been proposed for multiple comparison testing (Daniel, 2000).

A subtle approach to test for multiple comparisons and validate the Friedman test results is the post-hoc test according to Conover (Conover, 1999). Our resulting p-values are controlled by a moderately stringent family-wise error rate (FWER) procedure called FDR. This approach was applied to avoid the rate of Type 1 errors in null hypothesis testing, thereby preventing the problem of incorrect rejections (i.e. false discoveries). FDR-controlling processes have a greater power than the Bonferroni correction at the cost of increased occurrences of Type 1 errors (Ashby, 2011).

Both the Friedman test and the Conover's post-hoc test have been performed in the R statistical computing environment using the PMCMR package (Pohlert, 2014).

4 Results

This part presents all our findings. In EPI, the statistical significance of the average β-values and mean peak values of the average responses was evaluated. Statistical testing of the results in InI was not performed, as explained hereinafter.

4.1 EPI study

Below, the effects of different stimulus rates in EPI are demonstrated. All results are visualized on the cortical surface.

Before selecting a suitable statistical test, we applied the Kolmogorov-Smirnov goodness-of-fit hypothesis test to determine whether the mean β-values and the mean peak values of average time-series come from a standard normal distribution, i.e. $\mathcal{N}(0, 1)$. The rejection criterion was set at the 5% significance level (p-value = 0.05) with the null hypothesis that the data are normally distributed. As listed in Table 6, most of the values are not normally distributed.

	0.3 Hz	1.0 Hz	3.0 Hz	6.0 Hz	9.0 Hz	12.0 Hz
Mean β-values (S1)	**0.0551**	0.0152	0.0078	0.0066	0.0005	0.0042
Mean β-values (S2)	0.0083	0.0028	0.0036	0.0125	0.0029	0.0221
Peak response values (S1)	0.0039	0.0014	0.0016	0.0070	0.0003	0.0010
Peak response values (S2)	0.0016	0.0046	0.0050	0.0042	0.0038	0.0022

Table 6. Results of the Kolmogorov-Smirnov test for normality. Only one p-value complies with the criterion for standard normal distribution (in bold).

4.1.1 Cortical location of the main responses

The locations of brain responses on the cortical surface were obtained using two toolboxes for fMRI analysis, namely the dSPM and MNE packages.

Based on the Conover's post-hoc test of the mean peak values of the average time-series and the mean β-values for area S1, it was assumed that the strongest cortical brain activations were generated at the stimulation rate of 3 or 6 Hz. The differences in activations for the 3Hz or 6Hz conditions can be seen in Fig. 12. In Fig. 13, we can observe the anatomical locations of the cortical activations in Talairach space (for more information, see `www.neurosynth.org`).

4.1.2 Average response strength

The group average brain responses obtained from the EPI experiment are shown in Fig. 14. Table 7 lists the mean values of the group average time-courses for both somatosensory areas.

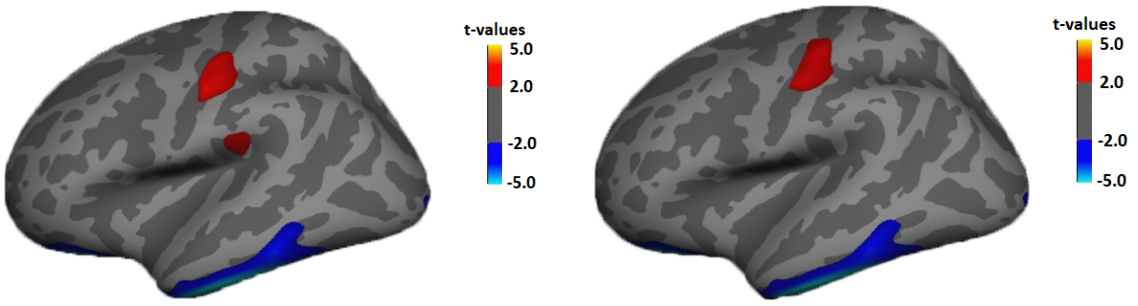

(a) (b)

Figure 12: Visualization of group-average cortical activations in area S1 (upper red cluster) and S2 (lower red cluster) for the (a) 3Hz condition and (b) 6Hz condition. Here, the t-values are found in the interval $[-5 \;\; 5]$, and thresholded at $[-2 \;\; 2]$. Blue colour in the inferior temporal lobe indicates that baseline activity is greater at rest than during task blocks.

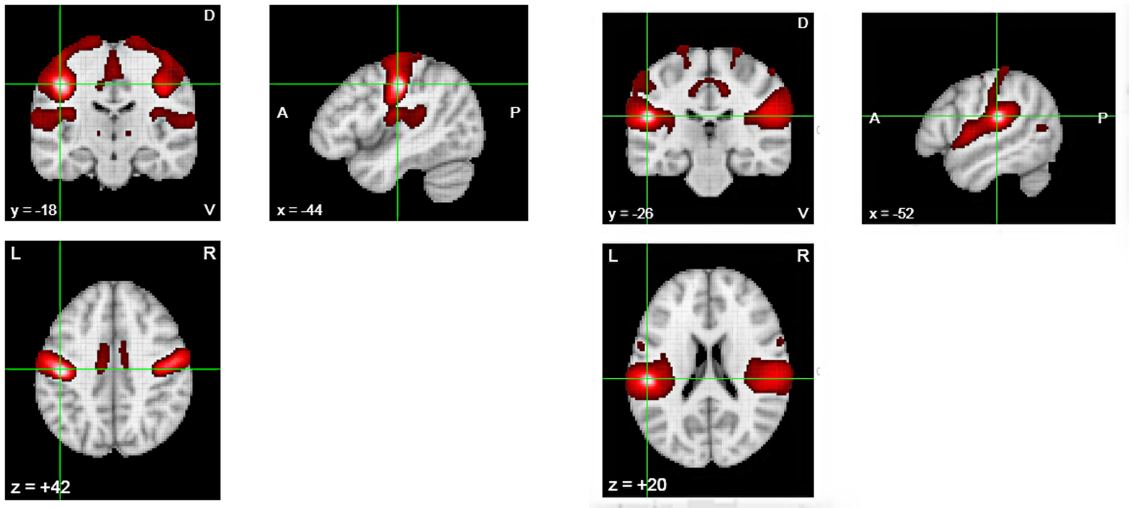

(a) (b)

Figure 13: Talairach coordinates [x, y, z] of the cortical responses at the 3Hz condition in (a) area S1 $[-44.42, -18.59, 41.02]$ and (b) area S2 $[-51.26, -25.59, 19.36]$.

A Friedman test was performed to assess the statistical significance of average β-values and mean peak values of average responses. Tables 13 and 14 list the subject-wise average β-values for all conditions in either of the cortical areas. Tables 15 and 16 list the subject-wise mean peak values of the average time-series for all subjects across all conditions in both cortical areas.

Tables 8, 9, 10 and 11 list the p-values obtained from the Conover's post-hoc test. All p-values were FDR-corrected for multiple comparisons. A non-parametric Friedman test of differences among repeated measures across average β-values in area S1 was conducted and rendered a $\chi^2(5)$ value of 23.37, which was significant ($p < 0.05$, $p = 0.0003$). A post-hoc test by Conover was performed on this dataset.

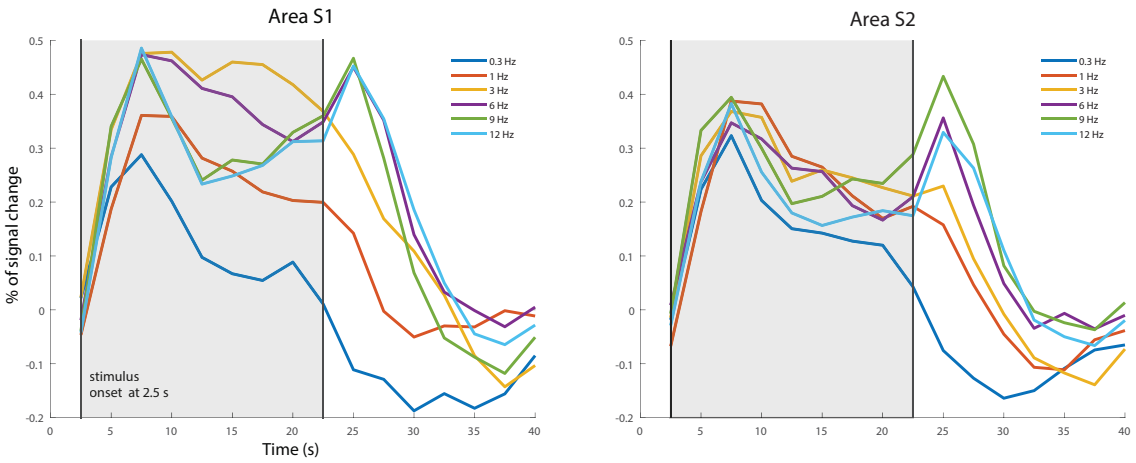

(a) (b)

Figure 14: Group average responses for all conditions in (a) area S1, and (b) area S2. Gray boxes indicate the period of 20s stimulation. $T_{\mathrm{R}} = 2.5\,\mathrm{s}$.

	0.3 Hz	1.0 Hz	3.0 Hz	6.0 Hz	9.0 Hz	12.0 Hz
S1	0.0082	0.1495	0.2701	0.2838	0.2285	0.2454
S2	0.0453	0.1400	0.1545	0.1796	0.2114	0.1651

Table 7. Condition-wise mean values of the average time-series across all subjects in both somatosensory areas for a period from 2.5 s to 35 s.

A non-parametric Friedman test of differences among repeated measures across average β-values in area S2 was conducted and rendered a $\chi^2(5)$ value of 5.2, which was insignificant ($p > 0.05$, $p = 0.392$). A post-hoc test by Conover was performed on this dataset.

A non-parametric Friedman test of differences among repeated measures across

	0.3 Hz	1.0 Hz	3.0 Hz	6.0 Hz	9.0 Hz
1.0 Hz	0.017	–	–	–	–
3.0 Hz	**0.0000003**	**0.001**	–	–	–
6.0 Hz	**0.0000081**	0.014	0.312	–	–
9.0 Hz	**0.00001**	0.002	0.246	0.847	–
12.0 Hz	**0.000029**	0.040	0.131	0.649	0.749

Table 8. P-values from the Conover's post-hoc test across average β-values for S1.

	0.3 Hz	1.0 Hz	3.0 Hz	6.0 Hz	9.0 Hz
1.0 Hz	0.13	–	–	–	–
3.0 Hz	0.13	0.94	–	–	–
6.0 Hz	0.14	0.94	0.94	–	–
9.0 Hz	0.13	1.00	0.94	0.94	–
12.0 Hz	0.21	0.94	0.94	0.94	0.94

Table 9. *P*-values from the Conover's post-hoc test across average β-values for S2.

mean peak values of average responses in area S1 was conducted and rendered a $\chi^2(5)$ value of 15.03, which was significant ($p < 0.05$, $p = 0.0102$). A post-hoc test by Conover was performed on this dataset.

	0.3 Hz	1.0 Hz	3.0 Hz	6.0 Hz	9.0 Hz
1.0 Hz	0.03918	–	–	–	–
3.0 Hz	**0.00025**	0.07	–	–	–
6.0 Hz	**0.00066**	0.197	0.759	–	–
9.0 Hz	**0.00098**	0.291	0.537	0.784	–
12.0 Hz	**0.00098**	0.291	0.537	0.784	1.000

Table 10. *P*-values from the Conover's post-hoc test across mean peak values of average responses in area S1.

A non-parametric Friedman test of differences among repeated measures across mean peak values of average responses in area S2 was conducted and rendered a $\chi^2(5)$ value of 1.09, which was insignificant ($p > 0.05$, $p = 0.955$). A post-hoc test by Conover was performed on this dataset.

	0.3 Hz	1.0 Hz	3.0 Hz	6.0 Hz	9.0 Hz
1.0 Hz	0.99	–	–	–	–
3.0 Hz	1.00	0.99	–	–	–
6.0 Hz	0.99	1.00	0.99	–	–
9.0 Hz	0.99	1.00	0.99	1.00	–
12.0 Hz	1.00	1.00	0.99	1.00	1.00

Table 11. *P*-values from the Conover's post-hoc test across mean peak values of average responses in area S2.

Figure 15 shows the statistical significance of average β-values and mean peak values of the average responses. In Table 12, the group averages of the mean β-values and the mean peak values of average responses are listed.

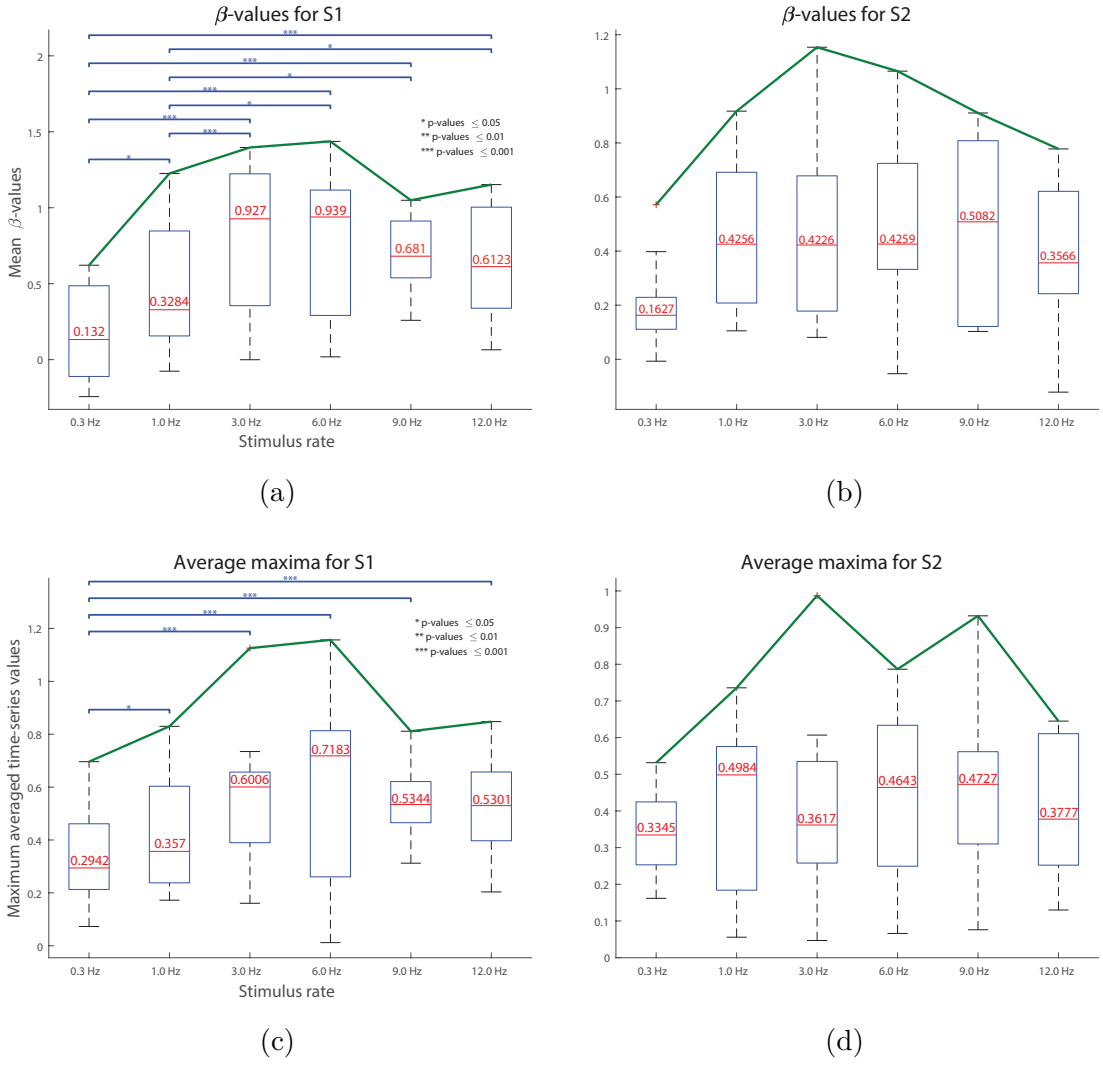

Figure 15: (a, b) Group ($N = 10$) mean β-values and the mean peak values of average time-series for the primary brain response in area S1. (c, d) Group ($N = 10$) mean β-values and the mean peak values of average time-series for the primary brain response in area S2. Medians indicated above the red lines. Statistically significant differences are shown with blue lines. Medians are indicated above the red lines.

4.2 InI pilot studies

Here, we demonstrate the outcomes of both InI pilot studies. In addition, the visualization of cortical responses is provided with an illustration of the signal intensity distribution over one slice.

4.2.1 Cortical location of the main responses in study 1 & 2

The BOLD signal t-statistics are visualized over the whole brain volume in Fig. 16. The presented results from InI study 1 were obtained from the event type with

	0.3 Hz	1.0 Hz	3.0 Hz	6.0 Hz	9.0 Hz	12.0 Hz
Mean β-values (S1)	0.1603	0.4887	0.8140	0.7802	0.6852	0.6412
Mean β-values (S2)	0.2053	0.4584	0.4771	0.4745	0.5047	0.3975
Peak response values (S1)	0.3272	0.4315	0.5866	0.5981	0.5392	0.5298
Peak response values (S2)	0.3412	0.4197	0.4083	0.4342	0.4605	0.4012

Table 12. Group average values of the mean β-values and the mean peak values of average responses in both somatosensory areas.

6-bursts (the 3-burst and single-event conditions yielded too weak brain responses). In the visualization of the results from InI study 2, the data was obtained from the event type with 12 consecutive movements, as we had assumed that this condition would yield the strongest brain responses.

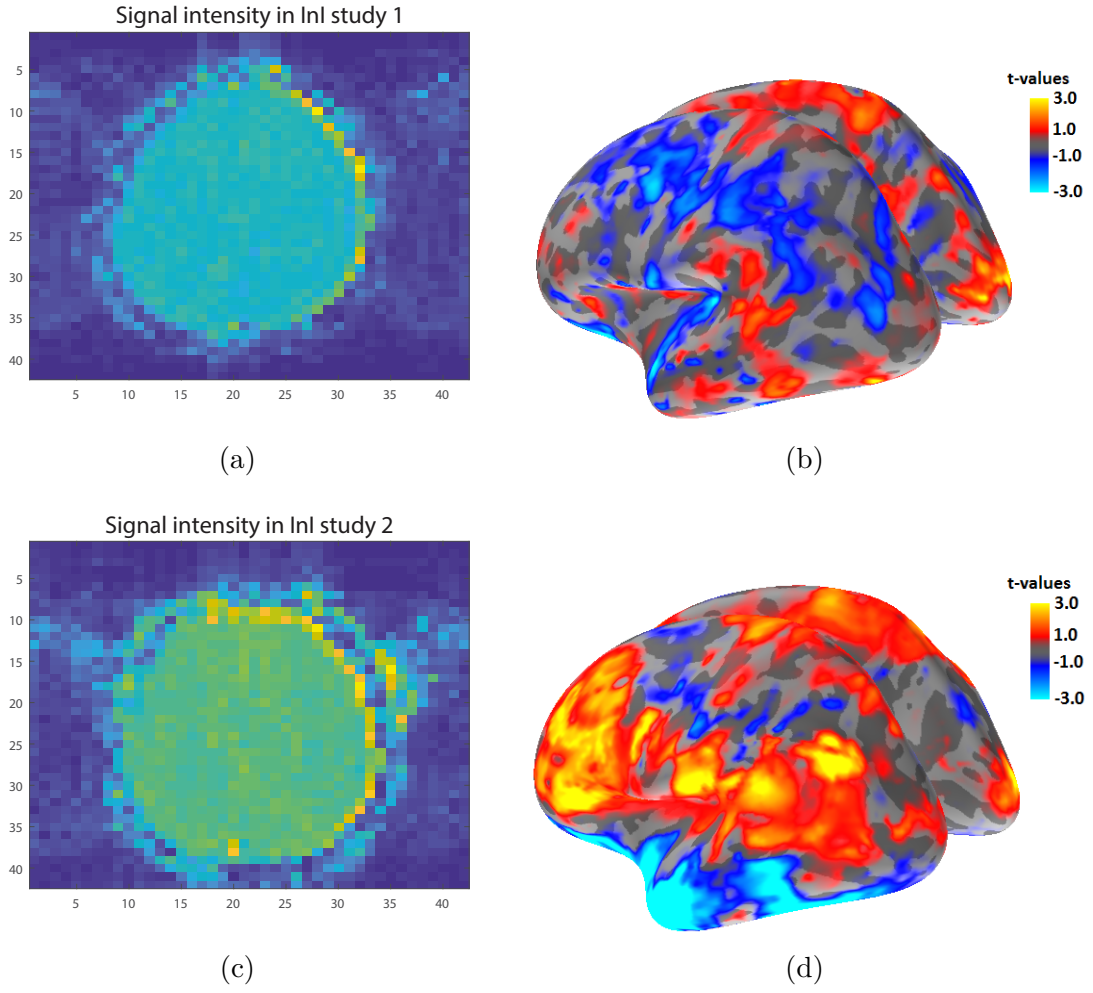

Figure 16: *Upper row*: InI pilot study 1, *lower row*: InI pilot study 2. (a, c) Signal intensity over a slice at one time point. (b, d) Visualization of InI dSPM t-statistics of the BOLD signal over the whole brain at 5 s after the stimulus onset.

5 Discussion

The results of this study provide an understanding of how different settings of stimulus parameters affect proprioceptive stimulation efficiency in fMRI with two imaging sequences. As reported in a previous MEG study (Piitulainen et al., 2015), we hypothesized that the optimal stimulus rate for evoking proprioceptive responses would be found within the upper limits of natural movement, ranging between 3 and 6 Hz. Moreover, we assumed that the increased sampling rate of InI would allow for tracking the shape of the BOLD response evoked by proprioceptive stimulation in area S1.

Apart from discussing all obtained results, this section also provides suggestions for potential improvements in the design of the conducted experiments.

5.1 EPI study

The principal purpose of the EPI study was to elucidate, at which stimulus rate one can obtain the strongest BOLD response to proprioceptive stimulation of the right upper index finger.

5.1.1 Cortical location of the main responses

The most prominent responses were found at stimulation rates 3Hz and 6 Hz, as shown in Fig. 12. The clusters of activation were present in area S1 at a threshold $t = 2$ at both these rates, while only in the case of the 3 Hz condition, significant activations were found in area S2 as well.

5.1.2 Average response strength

In echo-planar imaging, we applied a set of stimulation rates ranging from 0.3—12 Hz. In both areas (S1 and S2), we have obtained promising results with respect to the hemodynamic response shape and return to baseline.

In both brain ROIs, the BOLD responses reached the baseline at approximately 12 s after stimulus onset. Interestingly enough, secondary peak activity can be observed in both brain areas (Fig. 14), followed by a steep drop in the signal level. These stimulus offset responses (observed also in electrophysiological recordings) are present only at high stimulus rates, which is why this effect can be explained either by habituation phenomena or a gradual proprioceptive mismatch in the prediction of consecutive movements. This observation infers that the effect of stimulus rate may vanish at high rates since the brain perceives such stimuli as vibrations instead.

Based on the Conover's post-hoc test results, we efficiently assessed the statistical significance of β-values, and the mean peak response values of average responses. The results of the post-hoc assessment test are denoted by lines of statistical significance in figures 15a and 15c.

As we can see in Table 12, in area S1, the highest mean β-value is yielded by the 3Hz condition ($\mu = 0.8140$) followed by the 6Hz condition ($\mu = 0.7802$), while in area S2, there were no statistically significant activations found. These results are also confirmed by the blue lines indicating statistical importance.

According to the mean peak values of average time-series, the most significant set of activations occurred in area S1 at the 6Hz condition ($\mu = 0.5981$), and in the 3Hz condition ($\mu = 0.5866$). In area S2, there were no statistically significant activations detected.

5.2 InI pilot studies

We applied InI with the intention to sample the main BOLD response in S1 at a higher time precision than in EPI. In addition to tracking the magnitude of brain responses to varying rate of stimulation, we aimed at observing the effect of randomized stimulus duration at subsequent trial onsets.

5.2.1 Cortical location of the main responses in study 1 & 2

In the first InI pilot study, the order of stimulus onsets was not randomized at all (each stimulus was followed by a 12s rest period), which did not yield significant activations in the expected brain areas (S1 and S2). In Fig. 16b, only noise can be seen. We assumed that the activation patterns in the visual cortical areas were caused by stimulus-locked visual contamination.

Randomization of the stimulus onset was done in InI pilot study 2. However, no significant outcomes were obtained by stimulation with modified parameters either (Fig. 16d).

Nevertheless, in both InI pilot studies we only obtained random noise and artifacts hindering the acquisition of a high-quality signal. These misrepresentations of the anatomical structures and voxel-level signal mismatches were caused by motion, wrap-around artefacts (Fig. 16a and 16c), and scanner noise interfering with brain activations during fMRI. The subjects did not report any discomfort during the functional scans.

5.3 Limitations and future prospects

While the EPI experiment produced evident results with clear effects, the main insufficiencies in our InI pilot studies consisted of low sample size. However, our aim was to collect individual data, whence no group average analysis could be performed.

Another problem is reflected in the relatively high noise level present in the InI data. The functional images in InI were slightly obscured by motion artifacts, which cannot be compensated for, as algorithms for the removal of such confounds are yet to be developed. In addition, magnetic inhomogeneities and non-optimal stimulation parameters (trigger timings, jitter setup, stimulus variability), and habituation effects contributed to the image distortions.

Irrespective of non-optimal stimulation parameters, there are numerous technical obstacles that remain to be resolved. During our scans, the FOV could not be tilted nor resized in any encoding direction to include solely the brain ROIs (areas S1, S2, and the cerebellum). Thus, the image spatial resolution in these brain areas was somewhat hampered.

Obviously, future studies should pay attention to the optimization of stimulation parameters (randomized stimulus rate, randomized stimulus duration) in MR InI. Moreover, habituation phenomena should be studied more carefully with respect to minimizing their effects. The impact of stimulus duration, rate of stimulation, inter-stimulus interval and its asynchronicity on the brain activations should be further scrutinized as well. Also, the effects of movement range should be tested on different parts of the limbs, and a method for motion artifact compensation needs to be created.

In order to enhance stimulation efficiency, several adjustments must be tested to improve the measurement design. Firstly, the stimulus onset must be randomized even more rapidly. We set the stimuli within the interval of 4—12 s, which might have been inadequate. In InI, the interstimulus interval can be as short as 2 s and as long as 16 s, as instructed by Lin et al. (2012b).

Secondly, the stimuli do not need to be presented at integer multiples of seconds. In the second InI pilot study, the values were presented as multiples of 500 ms, which could have possibly led to limitations in the total number of trials per run.

Thirdly, collecting more data across several subjects and calculating group averages could significantly increase the signal strength and enlarge the visualized clusters of brain activations.

Next, to observe whether we can get at least some reasonable results using InI, it might be useful to test the experimental setup in regular EPI studies with the same ERD as used in InI.

Last, adding visual stimuli to the current design setup could show us whether the observed patterns of activation are sheer noise and whether this protocol design allows for obtaining any activations at all.

6 Conclusions

The summary of results obtained from all our experiments can be divided into two parts. First, the EPI experiment was appropriately designed and we were able to find the optimal stimulation rate (3—6 Hz). Secondly, we did not succeed in finding the optimum parameters for proprioceptive stimulation in either of the InI studies.

Answering the research questions Q_1 and Q_2, we can state the following:

A_1: In line with the previous MEG result (Piitulainen et al., 2015), the optimal stimulation in EPI occurred at the interval of 3—6 Hz, which denotes the upper limits of natural movement.

A_2: The optimal stimulation parameters for InI remain to be clarified. Thorough testing needs to be performed in order to optimize the stimulation setup, and improvements can be expected also in the InI method itself.

Several details require special attention when aiming at successful proprioceptive stimulation, such as optimal positioning of the subject, device testing, limb fixation, acquisition length, number of trials, duration of stimulation, etc. fMRI with ultrafast InI is a relatively new technology that poses numerous challenges differing from those encountered in EPI.

There is an indisputable need for further experiments to be conducted with a larger sample size and modified stimulation parameters. Hopefully, these modifications will allow for relevant studies of proprioception. Potential future applications of our InI experimental design are also perceived in the connectivity analysis of the proprioceptive brain network as well as in clinical neurorehabilitation therapy.

Appendices

Subject	0.3 Hz	1.0 Hz	3.0 Hz	6.0 Hz	9.0 Hz	12.0 Hz
1	-0.2435	-0.005	0.1346	0.043	0.2589	0.2502
2	0.518	0.847	1.3458	0.917	1.0492	1.1524
3	-0.1991	0.2904	1.0957	0.961	0.9126	0.5204
4	0.6216	1.1618	1.3967	1.1082	0.9679	0.5294
5	0.4863	0.362	1.2233	1.2844	0.6105	1.0038
6	0.2846	0.6304	0.7024	0.626	0.6566	0.6951
7	0.2994	1.2257	1.1289	1.4369	0.8544	0.7524
8	-0.0202	-0.0761	0.3553	0.2911	0.5385	0.0648
9	-0.1107	0.156	0.0006	0.0183	0.2977	0.3384
10	-0.0332	0.2949	0.7582	1.1162	0.7054	1.1049

Table 13. Average β-values for area S1, rounded to 4 digits.

Subject	0.3 Hz	1.0 Hz	3.0 Hz	6.0 Hz	9.0 Hz	12.0 Hz
1	0.229	0.9175	1.1538	0.841	0.8916	0.621
2	0.1552	0.1538	0.081	-0.0021	0.1029	0.1284
3	0.1527	0.2274	0.1782	0.4835	0.9107	-0.1215
4	0.398	0.5828	0.6782	0.6317	0.8081	0.4229
5	0.2139	0.1053	0.2837	0.3683	0.1144	0.2653
6	0.5717	0.6915	0.5941	0.3534	0.3584	0.5994
7	0.1109	0.8469	0.8671	1.0653	0.7227	0.7488
8	-0.0071	0.2081	0.3226	0.3325	0.4729	0.2903
9	0.1703	0.3921	0.0893	-0.0533	0.1214	0.2424
10	0.0579	0.4591	0.5226	0.7244	0.5436	0.7778

Table 14. Average β-values for area S2, rounded to 4 digits.

Subject	0.3 Hz	1.0 Hz	3.0 Hz	6.0 Hz	9.0 Hz	12.0 Hz
1	0.0728	0.1723	0.1606	0.135	0.3123	0.2036
2	0.6962	0.6033	1.1256	0.7359	0.8113	0.8477
3	0.2886	0.2877	0.6195	0.7705	0.5837	0.5307
4	0.4613	0.83	0.7346	0.7007	0.621	0.5748
5	0.5649	0.2579	0.6515	0.8686	0.4708	0.6573
6	0.2129	0.4262	0.3897	0.2606	0.3903	0.3236
7	0.2998	0.7772	0.6568	0.8134	0.5741	0.5296
8	0.3635	0.2379	0.3851	0.0118	0.4654	0.3971
9	0.2176	0.5236	0.5608	0.5281	0.4946	0.5281
10	0.0942	0.1991	0.5817	1.1568	0.6685	0.706

Table 15. Mean peak values of average time-series for S1, rounded to 4 digits.

Subject	0.3 Hz	1.0 Hz	3.0 Hz	6.0 Hz	9.0 Hz	12.0 Hz
1	0.5316	0.7358	0.9873	0.7866	0.9321	0.6107
2	0.3161	0.1413	0.3023	0.0963	0.076	0.1299
3	0.2272	0.0557	0.0467	0.5769	0.6023	0.1952
4	0.3529	0.5315	0.4227	0.5746	0.5366	0.4396
5	0.3102	0.184	0.2004	0.2602	0.2461	0.2522
6	0.4247	0.5756	0.535	0.3539	0.4801	0.645
7	0.2531	0.6738	0.6069	0.7444	0.5616	0.6249
8	0.3533	0.3029	0.2579	0.0659	0.4652	0.3158
9	0.4807	0.5035	0.3287	0.2493	0.31	0.2706
10	0.1617	0.4933	0.3947	0.6336	0.3952	0.5282

Table 16. Mean peak values of average time-series for S2, rounded to 4 digits.

References

Abbruzzese, G., Trompetto, C., Mori, L., and Pelosin, E. Proprioceptive Rehabilitation of Upper Limb Dysfunction in Movement Disorders: A Clinical Perspective. *Frontiers in Human Neuroscience*, 8, 2014. ISSN 1662-5161. doi: 10.3389/fnhum.2014.00961. URL `http://journal.frontiersin.org/article/10.3389/fnhum.2014.00961/full`.

Alary, F., Doyon, B., Loubinoux, I., Carel, C., Boulanouar, K., Ranjeva, J. P., Celsis, P., and Chollet, F. Event-Related Potentials Elicited by Passive Movements in Humans: Characterization, Source Analysis, and Comparison to fMRI. *NeuroImage*, 8(4):377–390, Nov. 1998. ISSN 1053-8119. doi: 10.1006/nimg.1998.0377. URL `http://www.sciencedirect.com/science/article/pii/S1053811998903779`.

Ashby, F. G. *Statistical Analysis of fMRI Data*. The MIT Press, Cambridge, Mass, 1st edition, Mar. 2011. ISBN 978-0-262-01504-2.

Bandettini, P. A. What's new in neuroimaging methods? *Annals of the New York Academy of Sciences*, 1156:260–293, Mar. 2009. ISSN 0077-8923. doi: 10.1111/j.1749-6632.2009.04420.x. URL `http://www.ncbi.nlm.nih.gov/pmc/articles/PMC2716071/`.

Baradaran, N., Tan, S. N., Liu, A., Ashoori, A., Palmer, S. J., Wang, Z. J., Oishi, M. M., and McKeown, M. J. Parkinson's Disease Rigidity: Relation to Brain Connectivity and Motor Performance. *Frontiers in Neurology*, 4, June 2013. ISSN 1664-2295. doi: 10.3389/fneur.2013.00067. URL `http://www.ncbi.nlm.nih.gov/pmc/articles/PMC3672800/`.

Bear, M. F., Connors, B. W., and Paradiso, M. A. *Neuroscience: Exploring the Brain*. Wolters Kluwer, Philadelphia, 4th edition, Feb. 2015. ISBN 978-0-7817-7817-6.

Belforte, G. and Eula, G. Design of an active–passive device for human ankle movement during functional magnetic resonance imaging analysis. *Proceedings of the Institution of Mechanical Engineers, Part H: Journal of Engineering in Medicine*, 226(1):21–32, Jan. 2012. ISSN 0954-4119. doi: 10.1177/0954411911426946. URL `http://journals.sagepub.com/doi/abs/10.1177/0954411911426946`.

Ben-Shabat, E., Matyas, T. A., Pell, G. S., Brodtmann, A., and Carey, L. M. The Right Supramarginal Gyrus Is Important for Proprioception in Healthy and Stroke-Affected Participants: A Functional MRI Study. *Frontiers in Neurology*, 6:248, 2015. doi: 10.3389/fneur.2015.00248.

Birn, R. M., Diamond, J. B., Smith, M. A., and Bandettini, P. A. Separating respiratory-variation-related fluctuations from neuronal-activity-related fluctuations in fMRI. *NeuroImage*, 31(4):1536–1548, July 2006. ISSN 1053-8119. doi: 10.1016/j.neuroimage.2006.02.048. URL `http://www.sciencedirect.com/science/article/pii/S1053811906001248`.

Blatow, M., Reinhardt, J., Riffel, K., Nennig, E., Wengenroth, M., and Stippich, C. Clinical functional MRI of sensorimotor cortex using passive motor and sensory stimulation at 3 tesla. *Journal of Magnetic Resonance Imaging*, 34(2):429–437, Aug. 2011. ISSN 1522-2586. doi: 10.1002/jmri.22629. URL `http://onlinelibrary.wiley.com/doi/10.1002/jmri.22629/abstract`.

Boscolo Galazzo, I., Storti, S. F., Formaggio, E., Pizzini, F. B., Fiaschi, A., Beltramello, A., Bertoldo, A., and Manganotti, P. Investigation of brain hemodynamic changes induced by active and passive movements: A combined arterial spin labeling–BOLD fMRI study. *Journal of Magnetic Resonance Imaging*, 40(4):937–948, Oct. 2014. ISSN 1522-2586. doi: 10.1002/jmri.24432. URL `http://onlinelibrary.wiley.com/doi/10.1002/jmri.24432/abstract`.

Carel, C., Loubinoux, I., Boulanouar, K., Manelfe, C., Rascol, O., Celsis, P., and Chollet, F. Neural Substrate for the Effects of Passive Training on Sensorimotor Cortical Representation: A Study with Functional Magnetic Resonance Imaging in Healthy Subjects. *Journal of Cerebral Blood Flow & Metabolism*, 20(3):478–484, Mar. 2000. ISSN 0271-678X. doi: 10.1097/00004647-200003000-00006. URL http://journals.sagepub.com/doi/abs/10.1097/00004647-200003000-00006.

Chang, W.-T., Nummenmaa, A., Witzel, T., Ahveninen, J., Huang, S., Tsai, K. W.-K., Chu, Y.-H., Polimeni, J. R., Belliveau, J. W., and Lin, F.-H. Whole-head rapid fMRI acquisition using echo-shifted magnetic resonance inverse imaging. *NeuroImage*, 78:325–338, Sept. 2013. ISSN 1053-8119. doi: 10.1016/j.neuroimage.2013.03.040. URL http://www.sciencedirect.com/science/article/pii/S1053811913002899.

Ciccarelli, O., Toosy, A. T., Marsden, J. F., Wheeler-Kingshott, C. M., Sahyoun, C., Matthews, P. M., Miller, D. H., and Thompson, A. J. Identifying brain regions for integrative sensorimotor processing with ankle movements. *Experimental Brain Research*, 166(1):31–42, Sept. 2005. ISSN 0014-4819, 1432-1106. doi: 10.1007/s00221-005-2335-5. URL https://link.springer.com/article/10.1007/s00221-005-2335-5.

Cohen, M. S. and Schmitt, F. Echo planar imaging before and after fMRI: A personal history. *NeuroImage*, 62(2):652–659, Aug. 2012. ISSN 1053-8119. doi: 10.1016/j.neuroimage.2012.01.038. URL http://www.sciencedirect.com/science/article/pii/S1053811912000559.

Conover, W. J. *Practical Nonparametric Statistics, 3rd.* Wiley, New York, 3rd edition, Dec. 1999. ISBN 978-0-471-16068-7.

Dale, A. M. and Buckner, R. L. Selective averaging of rapidly presented individual trials using fMRI. *Human Brain Mapping*, 5(5):329–340, Jan. 1997. ISSN 1097-0193. doi: 10.1002/(SICI)1097-0193(1997)5:5<329::AID-HBM1>3.0.CO;2-5. URL http://onlinelibrary.wiley.com/doi/10.1002/(SICI)1097-0193(1997)5:5<329::AID-HBM1>3.0.CO;2-5/abstract.

Daniel, W. W. *Applied Nonparametric Statistics.* Cengage Learning, Australia; Pacific Grove, CA, 2nd edition, June 2000. ISBN 978-0-534-38194-3.

de Zwart, J. A., Ledden, P. J., van Gelderen, P., Bodurka, J., Chu, R., and Duyn, J. H. Signal-to-noise ratio and parallel imaging performance of a 16-channel receive-only brain coil array at 3.0 Tesla. *Magnetic Resonance in Medicine*, 51(1):22–26, Jan. 2004. ISSN 1522-2594. doi: 10.1002/mrm.10678. URL http://onlinelibrary.wiley.com/doi/10.1002/mrm.10678/abstract.

Deshpande, G., Sathian, K., and Hu, X. Effect of hemodynamic variability on Granger causality analysis of fMRI. *NeuroImage*, 52(3):884–896, Sept. 2010. ISSN 1053-8119. doi: 10.1016/j.neuroimage.2009.11.060. URL http://www.sciencedirect.com/science/article/pii/S1053811909012464.

D'Esposito, M., Zarahn, E., and Aguirre, G. K. Event-related functional MRI: implications for cognitive psychology. *Psychological Bulletin*, 125(1):155–164, Jan. 1999. ISSN 0033-2909.

Deuschl, G., Lücking, C. H., and Schenck, E. Hand muscle reflexes following electrical stimulation in choreatic movement disorders. *Journal of Neurology, Neurosurgery & Psychiatry*, 52(6):755–762, June 1989. ISSN 0022-3050, 1468-330X. doi: 10.1136/jnnp.52.6.755. URL http://jnnp.bmj.com/content/52/6/755.

Dinomais, M., Minassian, A. T., Tuilier, T., Delion, M., Wilke, M., N'guyen, S., Richard, I., Aubé, C., and Menei, P. Functional Mri comparison of passive and active movement: possible inhibitory role of supplementary motor area. *Neuroreport*, 20(15):1351–1355, Oct. 2009. ISSN 0959-4965. doi: 10.1097/WNR.0b013e328330cd43. URL http://insights.ovid.com/pubmed?pmid=19734813.

Donaldson, D. I. Parsing brain activity with fMRI and mixed designs: what kind of a state is neuroimaging in? *Trends in Neurosciences*, 27(8):442–444, Aug. 2004. ISSN 0166-2236, 1878-108X. doi: 10.1016/j.tins.2004.06.001. URL http://www.cell.com/trends/neurosciences/abstract/S0166-2236(04)00168-7.

Edelman, R. R., Hesselink, J., and Zlatkin, M. *Clinical Magnetic Resonance Imaging: 3-Volume Set*. Saunders, Philadelphia, Pa, 3rd edition, Oct. 2005. ISBN 978-99960-19-49-4.

Enoka, R. *Neuromechanics of Human Movement-5th Edition*. Human Kinetics, Champaign, IL, 5th edition, Mar. 2015. ISBN 978-1-4504-5880-1.

Francis, S., Lin, X., Aboushoushah, S., White, T. P., Phillips, M., Bowtell, R., and Constantinescu, C. S. fMRI analysis of active, passive and electrically stimulated ankle dorsiflexion. *NeuroImage*, 44(2):469–479, Jan. 2009. ISSN 1053-8119. doi: 10.1016/j.neuroimage.2008.09.017. URL http://www.sciencedirect.com/science/article/pii/S1053811908009877.

Fu, Y., Zhang, Q., Zhang, J., and Zhang, Y. T. Comparative Functional MRI Study to Assess Brain Activation Upon Active and Passive Finger Movements in Patients with Cerebral Infarction. *European Neurology*, 73(1-2):13–19, 2015. ISSN 0014-3022, 1421-9913. doi: 10.1159/000366099. URL http://www.karger.com/Article/Abstract/366099.

Glover, G. H. Overview of Functional Magnetic Resonance Imaging. *Neurosurgery clinics of North America*, 22(2):133–139, Apr. 2011. ISSN 1042-3680. doi: 10.1016/j.nec.2010.11.001. URL http://www.ncbi.nlm.nih.gov/pmc/articles/PMC3073717/.

Griswold, M. A., Jakob, P. M., Heidemann, R. M., Nittka, M., Jellus, V., Wang, J., Kiefer, B., and Haase, A. Generalized autocalibrating partially parallel acquisitions (GRAPPA). *Magnetic Resonance in Medicine*, 47(6):1202–1210, June 2002. ISSN 1522-2594. doi: 10.1002/mrm.10171. URL http://onlinelibrary.wiley.com/doi/10.1002/mrm.10171/abstract.

Guzzetta, A., Staudt, M., Petacchi, E., Ehlers, J., Erb, M., Wilke, M., Krägeloh-Mann, I., and Cioni, G. Brain Representation of Active and Passive Hand Movements in Children. *Pediatric Research*, 61(4):485–490, Apr. 2007. ISSN 0031-3998. doi: 10.1203/pdr.0b013e3180332c2e. URL http://www.nature.com/pr/journal/v61/n4/full/pr200794a.html?foxtrotcallback=true.

Hinkley, L. B., Krubitzer, L. A., Nagarajan, S. S., and Disbrow, E. A. Sensorimotor Integration in S2, PV, and Parietal Rostroventral Areas of the Human Sylvian Fissure. *Journal of Neurophysiology*, 97(2):1288–1297, Feb. 2007. ISSN 0022-3077, 1522-1598. doi: 10.1152/jn.00733.2006. URL http://jn.physiology.org/content/97/2/1288.

Hämäläinen, M., Hari, R., Ilmoniemi, R. J., Knuutila, J., and Lounasmaa, O. V. Magnetoencephalography—theory, instrumentation, and applications to noninvasive studies of the working human brain. 1993. ISSN 0034-6861 (printed). doi: 10.1103/revmodphys.65.413. URL https://aaltodoc.aalto.fi:443/handle/123456789/18757.

Hollander, M. and Wolfe, D. A. *Nonparametric Statistical Methods*. Wiley-Interscience, New York, 2nd edition, Jan. 1999. ISBN 978-0-471-19045-5.

Huettel, S. A., Song, A. W., and McCarthy, G. *Functional Magnetic Resonance Imaging*. Sinauer, Sept. 2014. ISBN 978-0-87893-627-4.

Hung, Y.-C. and Meredith, G. S. Influence of dual task constraints on gait performance and bimanual coordination during walking in children with unilateral Cerebral Palsy. *Research in Developmental Disabilities*, 35(4):755–760, Apr. 2014. ISSN 0891-4222. doi: 10.1016/j.ridd.2014.01.024. URL http://www.sciencedirect.com/science/article/pii/S0891422214000389.

Iandolo, R., Marre, I., Bellini, A., Bommarito, G., Oesingmann, N., Fleysher, L., Levrero, F., Mancardi, G., Casadio, M., and Inglese, M. Neural correlates of ankle movements during different motor tasks: A feasibility study. In *2015 37th Annual International Conference of the IEEE Engineering in Medicine and Biology Society (EMBC)*, pages 4679–4682, Aug. 2015. doi: 10.1109/EMBC.2015.7319438.

Katz-Leurer, M., Rotem, H., and Meyer, S. Effect of concurrent cognitive tasks on temporo-spatial parameters of gait among children with cerebral palsy and typically developed controls. *Developmental Neurorehabilitation*, 17(6):363–367, Dec. 2014. ISSN 1751-8423. doi: 10.3109/17518423.2013.810676. URL http://dx.doi.org/10.3109/17518423.2013.810676.

Kellman, P. and McVeigh, E. R. Ghost artifact cancellation using phased array processing. *Magnetic Resonance in Medicine*, 46(2):335–343, Aug. 2001. ISSN 1522-2594. doi: 10.1002/mrm.1196. URL http://onlinelibrary.wiley.com/doi/10.1002/mrm.1196/abstract.

Krüger, G. and Glover, G. H. Physiological noise in oxygenation-sensitive magnetic resonance imaging. *Magnetic Resonance in Medicine*, 46(4):631–637, Oct. 2001. ISSN 1522-2594. doi: 10.1002/mrm.1240. URL http://onlinelibrary.wiley.com/doi/10.1002/mrm.1240/abstract.

Lee, C. C., Jack, C. R., and Riederer, S. J. Mapping of the central sulcus with functional MR: active versus passive activation tasks. *American Journal of Neuroradiology*, 19(5):847–852, May 1998. ISSN 0195-6108, 1936-959X. URL http://www.ajnr.org/content/19/5/847.

Lee, M. Y., Kim, S. H., Choi, B. Y., Chang, C. H., Ahn, S. H., and Jang, S. H. Functional MRI finding by proprioceptive input in patients with thalamic hemorrhage. *NeuroRehabilitation*, 30(2):131–136, Jan. 2012. ISSN 1053-8135. doi: 10.3233/NRE-2012-0736. URL http://content.iospress.com/articles/neurorehabilitation/nre00736.

Lin, F.-H., Wald, L. L., Ahlfors, S. P., Hämäläinen, M. S., Kwong, K. K., and Belliveau, J. W. Dynamic magnetic resonance inverse imaging of human brain function. *Magnetic Resonance in Medicine*, 56(4):787–802, Oct. 2006. ISSN 1522-2594. doi: 10.1002/mrm.20997. URL http://onlinelibrary.wiley.com/doi/10.1002/mrm.20997/abstract.

Lin, F.-H., Witzel, T., Mandeville, J. B., Polimeni, J. R., Zeffiro, T. A., Greve, D. N., Wiggins, G., Wald, L. L., and Belliveau, J. W. Event-related Single-shot Volumetric Functional Magnetic Resonance Inverse Imaging of Visual Processing. *NeuroImage*, 42(1):230–247, Aug. 2008. ISSN 1053-8119. doi: 10.1016/j.neuroimage.2008.04.179. URL http://www.ncbi.nlm.nih.gov/pmc/articles/PMC2659356/.

Lin, F.-H., Witzel, T., Chang, W.-T., Wen-Kai Tsai, K., Wang, Y.-H., Kuo, W.-J., and Belliveau, J. W. K-space reconstruction of magnetic resonance inverse imaging (K-InI) of human visuomotor systems. *NeuroImage*, 49(4):3086–3098, Feb. 2010. ISSN 1053-8119. doi: 10.1016/j.neuroimage.2009.11.016. URL http://www.sciencedirect.com/science/article/pii/S1053811909012002.

Lin, F.-H., Nummenmaa, A., Witzel, T., Polimeni, J. R., Zeffiro, T. A., Wang, F.-N., and Belliveau, J. W. Physiological Noise Reduction Using Volumetric Functional Magnetic Resonance Inverse Imaging. *Human brain mapping*, 33(12):2815–2830, Dec. 2012a. ISSN 1065-9471. doi: 10.1002/hbm.21403. URL http://www.ncbi.nlm.nih.gov/pmc/articles/PMC3586826/.

Lin, F.-H., Tsai, K. W. K., Chu, Y.-H., Witzel, T., Nummenmaa, A., Raij, T., Ahveninen, J., Kuo, W.-J., and Belliveau, J. W. Ultrafast inverse imaging techniques for fMRI. *NeuroImage*, 62(2):699–705, Aug. 2012b. ISSN 1053-8119. doi: 10.1016/j.neuroimage.2012.01.072. URL http://www.sciencedirect.com/science/article/pii/S1053811912000894.

Lin, F.-H., Ahveninen, J., Raij, T., Witzel, T., Chu, Y.-H., Jääskeläinen, I. P., Tsai, K. W.-K., Kuo, W.-J., and Belliveau, J. W. Increasing fMRI Sampling Rate Improves Granger Causality Estimates. *PLOS ONE*, 9(6):e100319, June 2014. ISSN 1932-6203. doi: 10.1371/journal.pone.0100319. URL http://journals.plos.org/plosone/article?id=10.1371/journal.pone.0100319.

Luca, A. D., Giannoni, P., Vernetti, H., Capra, C., Cassiano, C., Loguercio, L., Pisu, I., Gaito, F., Barone, L., Carioti, R., Lentino, C., Checchia, G., and casadio, m. Training the unimpaired arm improves the motion of the impaired arm and the sitting balance in chronic stroke survivors. *IEEE Transactions on Neural Systems and Rehabilitation Engineering*, PP(99):1–1, 2017. ISSN 1534-4320. doi: 10.1109/TNSRE.2016.2635806.

Mansfield, P. Multi-planar image formation using NMR spin echoes. *Journal of Physics C: Solid State Physics*, 10(3):L55, 1977. ISSN 0022-3719. doi: 10.1088/0022-3719/10/3/004. URL http://stacks.iop.org/0022-3719/10/i=3/a=004.

McDougall, M. P. and Wright, S. M. 64-channel array coil for single echo acquisition magnetic resonance imaging. *Magnetic Resonance in Medicine*, 54(2):386–392, Aug. 2005. ISSN 1522-2594. doi: 10.1002/mrm.20568. URL http://onlinelibrary.wiley.com/doi/10.1002/mrm.20568/abstract.

Meltzer, J. A., Negishi, M., and Constable, R. T. Biphasic hemodynamic responses influence deactivation and may mask activation in block-design fMRI paradigms. *Human Brain Mapping*, 29(4):385–399, Apr. 2008. ISSN 1097-0193. doi: 10.1002/hbm.20391. URL http://onlinelibrary.wiley.com/doi/10.1002/hbm.20391/abstract.

Menon, R. S., Luknowsky, D. C., and Gati, J. S. Mental chronometry using latency-resolved functional MRI. *Proceedings of the National Academy of Sciences of the United States of America*, 95(18):10902–10907, Sept. 1998. ISSN 0027-8424. URL http://www.ncbi.nlm.nih.gov/pmc/articles/PMC27993/.

Miezin, F. M., Maccotta, L., Ollinger, J. M., Petersen, S. E., and Buckner, R. L. Characterizing the Hemodynamic Response: Effects of Presentation Rate, Sampling Procedure, and the Possibility of Ordering Brain Activity Based on Relative Timing. *NeuroImage*, 11(6):735–759, June 2000. ISSN 1053-8119. doi: 10.1006/nimg.2000.0568. URL http://www.sciencedirect.com/science/article/pii/S1053811900905688.

Mima, T., Sadato, N., Yazawa, S., Hanakawa, T., Fukuyama, H., Yonekura, Y., and Shibasaki, H. Brain structures related to active and passive finger movements in man. *Brain: A Journal of Neurology*, 122 (Pt 10):1989–1997, Oct. 1999. ISSN 0006-8950.

Mintzopoulos, D., Khanicheh, A., Konstas, A. A., Astrakas, L. G., Singhal, A. B., Moskowitz, M. A., Rosen, B. R., and Tzika, A. A. Functional MRI of Rehabilitation in Chronic Stroke Patients Using Novel MR-Compatible Hand Robots. *The Open Neuroimaging Journal*, 2:94–101, Sept. 2008. ISSN 1874-4400. doi: 10.2174/1874440000802010094. URL http://www.ncbi.nlm.nih.gov/pmc/articles/PMC2695624/.

Ogawa, S., Lee, T. M., Kay, A. R., and Tank, D. W. Brain magnetic resonance imaging with contrast dependent on blood oxygenation. *Proceedings of the National Academy of Sciences of the United States of America*, 87(24):9868–9872, Dec. 1990. ISSN 0027-8424. URL http://www.ncbi.nlm.nih.gov/pmc/articles/PMC55275/.

Penny, W. D., Friston, K. J., Ashburner, J. T., Kiebel, S. J., and Nichols, T. E. *Statistical Parametric Mapping: The Analysis of Functional Brain Images*. Academic Press, Apr. 2011. ISBN 978-0-08-046650-7.

Petersen, S. E. and Dubis, J. W. The mixed block/event-related design. *Neuroimage*, 62 (2):1177–1184, Aug. 2012. ISSN 1053-8119. doi: 10.1016/j.neuroimage.2011.09.084. URL http://www.ncbi.nlm.nih.gov/pmc/articles/PMC3288695/.

Piitulainen, H., Bourguignon, M., Hari, R., and Jousmäki, V. MEG-compatible pneumatic stimulator to elicit passive finger and toe movements. *NeuroImage*, 112:310–317, May 2015. ISSN 1053-8119. doi: 10.1016/j.neuroimage.2015.03.006. URL http://www.sciencedirect.com/science/article/pii/S1053811915001810.

Pohlert, T. *The Pairwise Multiple Comparison of Mean Ranks Package (PMCMR). R-package.* Jan. 2014. URL http://CRAN.R-project.org/package=PMCMR.

Rosenkranz, K., Butler, K., Williamon, A., and Rothwell, J. C. Regaining Motor Control in Musician's Dystonia by Restoring Sensorimotor Organization. *Journal of Neuroscience*, 29(46): 14627–14636, Nov. 2009. ISSN 0270-6474, 1529-2401. doi: 10.1523/JNEUROSCI.2094-09.2009. URL http://www.jneurosci.org/content/29/46/14627.

Sahyoun, C., Floyer-Lea, A., Johansen-Berg, H., and Matthews, P. M. Towards an understanding of gait control: brain activation during the anticipation, preparation and execution of foot movements. *NeuroImage*, 21(2):568–575, Feb. 2004. ISSN 1053-8119. doi: 10.1016/j.neuroimage.2003.09.065. URL http://www.sciencedirect.com/science/article/pii/S105381190300644X.

Sodickson, D. K. and Manning, W. J. Simultaneous acquisition of spatial harmonics (SMASH): fast imaging with radiofrequency coil arrays. *Magnetic Resonance in Medicine*, 38(4):591–603, Oct. 1997. ISSN 0740-3194.

Szameitat, A. J., Shen, S., Conforto, A., and Sterr, A. Cortical activation during executed, imagined, observed, and passive wrist movements in healthy volunteers and stroke patients. *NeuroImage*, 62(1):266–280, Aug. 2012. ISSN 1053-8119. doi: 10.1016/j.neuroimage.2012.05.009. URL http://www.sciencedirect.com/science/article/pii/S1053811912004971.

Takahashi, C. D., Der-Yeghiaian, L., Le, V., Motiwala, R. R., and Cramer, S. C. Robot-based hand motor therapy after stroke. *Brain*, 131(2):425–437, Feb. 2008. ISSN 0006-8950. doi: 10.1093/brain/awm311. URL https://academic.oup.com/brain/article/131/2/425/406042/Robot-based-hand-motor-therapy-after-stroke.

Taylor, S. F., Stern, E. R., and Gehring, W. J. Neural Systems for Error Monitoring: Recent Findings and Theoretical Perspectives. *The Neuroscientist*, 13(2):160–172, Apr. 2007. ISSN 1073-8584. doi: 10.1177/1073858406298184. URL http://dx.doi.org/10.1177/1073858406298184.

Tie, Y., Suarez, R. O., Whalen, S., Radmanesh, A., Norton, I. H., and Golby, A. J. Comparison of blocked and event-related fMRI designs for pre-surgical language mapping. *NeuroImage*, 47 (Suppl 2):T107–T115, Aug. 2009. ISSN 1053-8119. doi: 10.1016/j.neuroimage.2008.11.020. URL http://www.ncbi.nlm.nih.gov/pmc/articles/PMC3036974/.

Van de Winckel, A., Klingels, K., Bruyninckx, F., Wenderoth, N., Peeters, R., Sunaert, S., Van Hecke, W., De Cock, P., Eyssen, M., De Weerdt, W., and Feys, H. How does brain activation differ in children with unilateral cerebral palsy compared to typically developing children, during active and passive movements, and tactile stimulation? An fMRI study. *Research in Developmental Disabilities*, 34(1):183–197, Jan. 2013. ISSN 0891-4222. doi: 10.1016/j.ridd.2012.07.030. URL http://www.sciencedirect.com/science/article/pii/S0891422212001977.

Veverka, T., Hluštík, P., Hok, P., Otruba, P., Zapletalová, J., Tüdös, Z., Krobot, A., and Kaňovský, P. Sensorimotor modulation by botulinum toxin A in post-stroke arm spasticity: Passive hand movement. *Journal of the Neurological Sciences*, 362:14–20, Mar. 2016. ISSN 0022-510X. doi: 10.1016/j.jns.2015.12.049. URL http://www.sciencedirect.com/science/article/pii/S0022510X15301143.

Vér, C., Emri, M., Spisák, T., Berényi, E., Kovács, K., Katona, P., Balkay, L., Menyhárt, L., Kardos, L., and Csiba, L. The Effect of Passive Movement for Paretic Ankle-Foot and Brain Activity in Post-Stroke Patients. *European Neurology*, 76(3-4):132–142, 2016. ISSN 0014-3022, 1421-9913. doi: 10.1159/000448033. URL http://www.karger.com/Article/Abstract/448033.

Ward, N. S., Brown, M. M., Thompson, A. J., and Frackowiak, R. S. J. Longitudinal Changes in Cerebral Response to Proprioceptive Input in Individual Patients after Stroke: An fMRI Study. *Neurorehabilitation and Neural Repair*, 20(3):398–405, Sept. 2006. ISSN 1545-9683. doi: 10.1177/1545968306286322. URL http://journals.sagepub.com/doi/abs/10.1177/1545968306286322.

Weiller, C., Jüptner, M., Fellows, S., Rijntjes, M., Leonhardt, G., Kiebel, S., Müller, S., Diener, H. C., and Thilmann, A. F. Brain Representation of Active and Passive Movements. *NeuroImage*, 4(2):105–110, Oct. 1996. ISSN 1053-8119. doi: 10.1006/nimg.1996.0034. URL http://www.sciencedirect.com/science/article/pii/S1053811996900348.

Wilke, M., Staudt, M., Juenger, H., Grodd, W., Braun, C., and Krägeloh-Mann, I. Somatosensory system in two types of motor reorganization in congenital hemiparesis: Topography and function. *Human Brain Mapping*, 30(3):776–788, Mar. 2009. ISSN 1097-0193. doi: 10.1002/hbm.20545. URL http://onlinelibrary.wiley.com/doi/10.1002/hbm.20545/abstract.